

Advanced SYNCOM

December 1962

MONTHLY PROGRESS REPORT

NASA Contract 5-2797
SSD 3020R

FACILITY FORM 602
N66-83661
(ACCESSION NUMBER)
83
(PAGES)
CL74568
(NASA CR OR TMX OR AD NUMBER)

(THRU)
NONE
(CODE)
(CATEGORY)

AEROSPACE GROUP
SPACE SYSTEMS DIVISION
HUGHES AIRCRAFT COMPANY
CULVER CITY, CALIFORNIA

HUGHES

HUGHES AIRCRAFT COMPANY

AEROSPACE GROUP

SPACE SYSTEMS DIVISION

CULVER CITY, CALIFORNIA

15 January 1963

SUBJECT: Advanced Syncom Monthly Report for December 1962

TO: Mr. Alton E. Jones
Program Manager, Syncom
Goddard Space Flight Center
Code 621
Greenbelt, Maryland

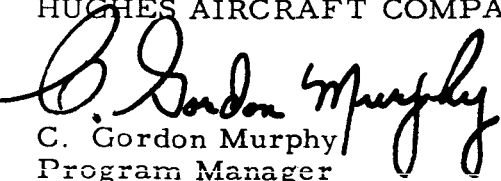
Attached are copies of the Advanced Syncom Monthly Progress Report for December 1962.

The phased-array antenna RF components were assembled with the antenna elements and array tests initiated using the RF power splitter and ferrite phase shifters to supply element excitation.

Final evaluation of bids for the hot gas system is under way and selection of the vendor for this system is expected early in January 1963.

System design studies have resulted in the selection of telemetry and command subsystem approaches which provide compatibility with Goddard standards for these systems.

HUGHES AIRCRAFT COMPANY


C. Gordon Murphy
Program Manager
Project Syncom

cc: H. E. Tetirick
Goddard Space Flight Center
Code 621
Greenbelt, Maryland

Advanced SYNCOM

December 1962

MONTHLY PROGRESS REPORT

-

*NASA Contract 5-2797
SSD 3020R*

AEROSPACE GROUP
SPACE SYSTEMS DIVISION
HUGHES AIRCRAFT COMPANY
CULVER CITY, CALIFORNIA

HUGHES

CONTENTS

	Page
1. INTRODUCTION	1-1
2. SYSTEM DESIGN STUDY	
Telemetry Subsystem	2-1
Command Subsystem	2-11
Orbit Analyses and Spacecraft Dynamics	2-12
Electrical Power Subsystem	2-13
System Reliability Studies	2-19
Test Equipment	2-20
References	2-28
3. ADVANCED TECHNOLOGICAL DEVELOPMENT	
Dual Mode Transponder	3-1
Traveling-wave Tube	3-9
Phased Array Transmitting Antenna	3-10
Collinear Array Receiving Antenna	3-20
Structure	3-28
Handling, Weight, and Balance Equipment	3-33
Hot Gas Reaction Jet Control Subsystem	3-38
Apogee Engine Liaison	3-45
4. NEW TECHNOLOGY	4-1
5. PROJECT REFERENCE REPORTS	5-1

1. INTRODUCTION

Under NASA Goddard Space Flight Center Contract NAS-5-2797, Hughes Aircraft Company is conducting feasibility studies and advanced technological development for an advanced, stationary, active repeater, communication satellite.

An Initial Project Development Plan, submitted to Goddard on 15 August 1962, reported the initial system feasibility studies and delineated technical approaches, the administrative plan, manpower requirements, schedule, and funding considerations appropriate for accomplishing the NASA contract objectives.

These monthly technical letter reports present the technical progress made during the reporting period, the critical problems or delays encountered, and the plans for the forthcoming reporting period.

Separate reports of schedule status are provided through biweekly PERT reports. Monthly financial management reports provide the funding status.

2. SYSTEM DESIGN STUDY

Studies of the Syncom II spacecraft system design during December consisted of updating the ascent guidance error estimates in accordance with the recently released Lockheed Missiles and Space Company final report of their Syncom II booster feasibility studies, consideration of thrust misalignment effects on spacecraft attitude, and consideration of telemetry and command systems performance and format.

A draft of the System Performance and Environmental Test Requirements Specification is being revised for submission to Goddard during the next reporting period. Two design reviews are scheduled for the first week in January. Results of these reviews will be reported in summary form in the next monthly report.

The electrical power subsystem design was revised to reflect incorporation of n-p cells which exhibit improved resistance to radiation over the p-n cells included in the design summary of the 15 August 1962 Initial Project Development Plan for Advanced Syncom.

TELEMETRY SUBSYSTEM

The telemetry subsystem design has been revised to reflect a pulse frequency modulation (PFM) system based upon NASA-Goddard Space Flight Center Standards for PFM (Reference 2-1). The system selected is a time division multiplexed system in which the signal information is carried in the form of the frequency of a subcarrier oscillator. In this system, the PFM encoder aboard the spacecraft is simple and reliable. The complexity in the system is transferred from the spacecraft to the ground stations where weight and power requirements do not penalize the design. A discussion of a means of implementing the Goddard format is presented later in this section.

One of the unique aspects of this system is a bank of contiguous band-pass filters used on the ground with a "greatest of" type detector to obtain a representation of the analog signal in a single burst to an accuracy of one part in one hundred. The output noise is then only the noise contained in one band of this comb filter and is thus only a small fraction of the input noise.

Several commutation rates are allowed in the NASA-PFM standards. However, real-time data processing by NASA is currently available only on the 50-channel-per-second system. This data rate appears adequate for Advanced Syncom and because of the desirability of having real-time data available, this particular mode will be used. The subcarrier center frequency is 10 kc and the deviation is ± 5 kc, resulting in minimum and maximum frequencies of 5 kc and 15 kc, respectively. About 150 channels are derived by using 10 PFM frames of 15 data channels per frame. A sixteenth channel in each frame is used for synchronization.

The PFM telemetry frame format is illustrated in Figure 2-1. The beginning of each frame is identified by the presence of the sync pulse with both a period and a frequency distinct from the remaining bursts in the frame. Each data channel burst is separated by a reference burst of known frequency. The frequency of the synchronization burst is specified to be 10 percent lower than the prescribed lower frequency edge of the data subcarrier band (i. e. , 5000 cps to 500 cps or 4500 cps) and the long term stability shall be better than 1 percent. Alternate frames employ a synchronization burst which is stepped in frequency to provide frame location information.

A 10-frame PFM telemetry sequence is illustrated in Figure 2-2. The sync channel frequencies for alternate frames are shown in Table 2-1. For the others which are between alternate frames, the frequency of the synchronization burst is 4500 cps.

Preliminary Analysis of Telemetry Subsystem

The following system parameters are assumed, based on measurements made on Syncom I:

<u>Spacecraft</u>	
Cable losses	0.13 db
Attenuator loss	1.50 db
Diplexer loss	0.70 db
Hybrid-balun loss	0.50 db
Antenna gain (worst case)	-3.20 db
Free space loss	167.4 db

<u>Ground Terminal</u>	
Antenna gain	25.10 db
Antenna mismatch loss	0.01 db
Line loss preceding preamp.	0.30 db
Filter loss	2.00 db
Receiving system noise figure	1.93 db
Galactic noise	1000°K

TABLE 2-1. SYNCHRONIZATION FREQUENCIES

Frame Number		Frequency Tolerance, \pm percent	Center Frequency, kc
Decimal	Binary		
0	000	7.6	5.30
1		1.0	4.50
2	001	6.2	6.50
3		1.0	4.50
4	010	5.2	7.70
5		1.0	4.50
6	011	4.5	8.90
7		1.0	4.50
8	100	4.0	10.10
9		1.0	4.50

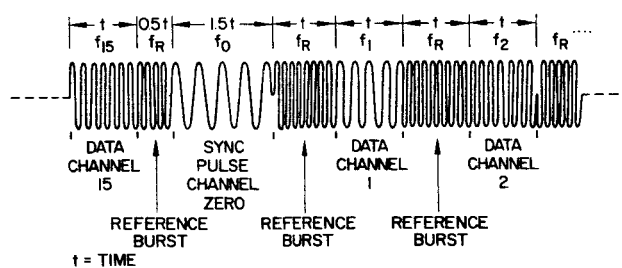


Figure 2-1. PFM Telemetry Frame Format

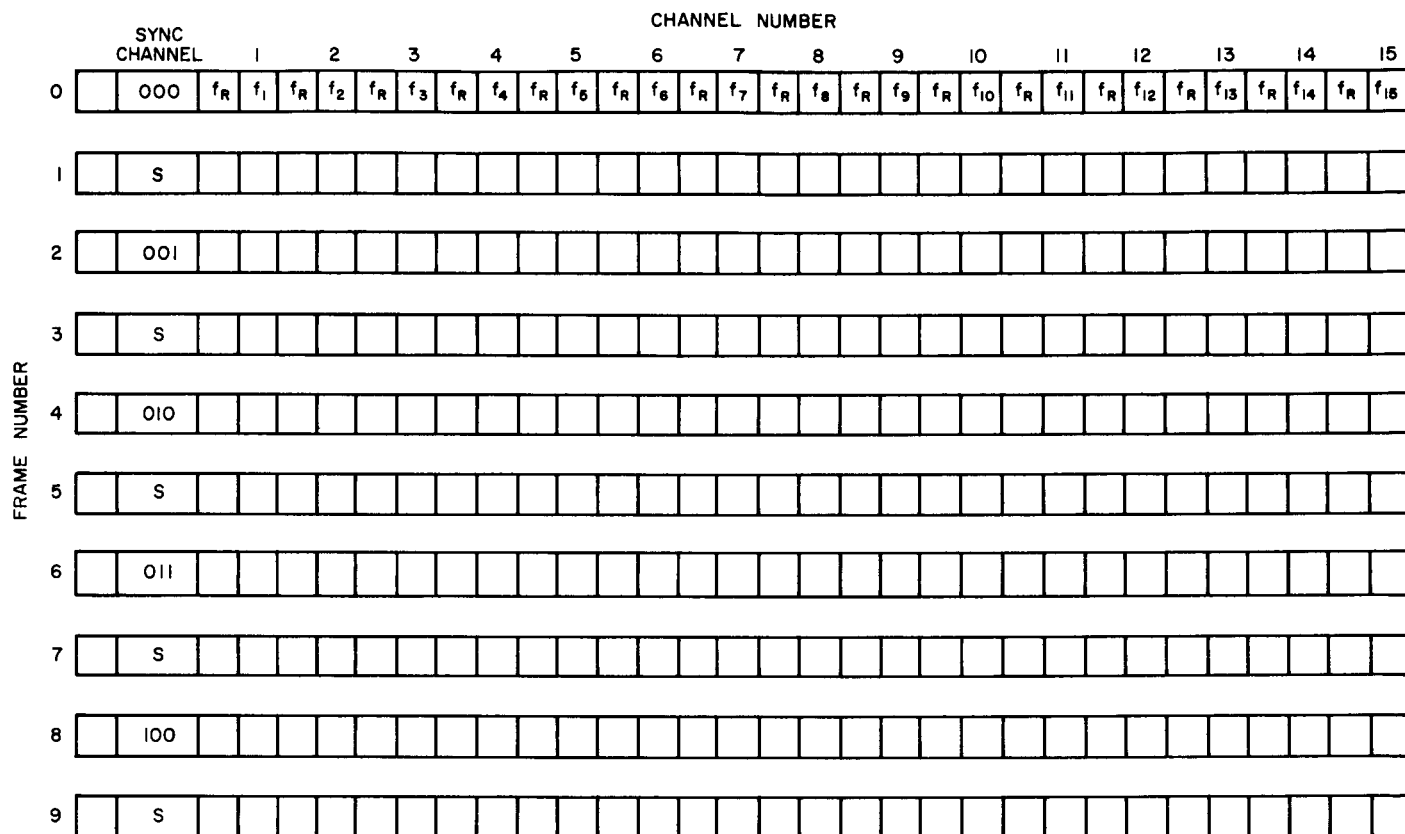


Figure 2-2. 10-Frame PFM Telemetry Sequence
Blank designations inferred by symmetry

The receiver noise temperature, referred to the input of the pre-amplifier, is determined as follows:

$$T_{in} = \frac{T_G}{L} + \frac{(L - 1)}{L} T_L + T_P \quad (2-1)$$

where

T_{in} = receiver noise temperature referred to input of the preamplifier, degrees K

T_G = Galactic noise temperature, degrees K

L = Attenuation power ratio = $\frac{\text{input power to attenuator}}{\text{output power from attenuator}}$

T_L = Ambient temperature of transmission line elements

T_P = Receiving system noise temperature = $(F-1) 290$

F = Receiver noise figure = 1.93 db

The attenuator power ratio, L , is made up of the sum of the filter loss and the line loss preceding the preamplifier (2.0 db + 0.3 db = 2.3 db). The ambient temperature of the transmission line is assumed to be 290°K.

$$T_P = (F - 1) 290 = (1.56 - 1) 290 = 162^\circ\text{K} \quad (2-2)$$

$$L = 2.3 \text{ db or a ratio of } 1.70/1$$

Therefore,

$$T_{in} = \frac{1000}{1.7} + \frac{(1.7 - 1)}{1.7} 290 + 162 = 870^\circ\text{K} \quad (2-3)$$

The noise spectral density, N_O , may now be determined

$$N_O = k T_{in} \quad (2-4)$$

where

N_O = noise spectral density

k = Boltzmann's constant = -228.6 db/°K/cps

$$10 \log N_O = -228.6 + 10 \log 870 = -199.2 \text{ dbw}$$

The net loss is determined by adding the losses and gains throughout the system.

<u>Losses</u>		<u>Gains</u>	
Cable loss	0.13 db	Ground antenna gain	25.1 db
Attenuator loss	1.50 db	Spacecraft antenna gain	-3.2 db
Diplexer loss	0.70 db	Total	21.9 db
Hybrid-balun loss	0.50 db		
Free space loss	167.40 db		
Ground mismatch loss	0.01 db		
Ground line losses	0.30 db		
Ground filter loss	2.00 db		
Total	172.54 db		

$$\text{Net loss} = 172.5 - 21.9 = 150.6 \text{ db}$$

A significant system parameter is the minimum power required at the spacecraft transmitter. One way to determine this power is to set a maximum filter selection error rate at the ground station filter bank and determine the signal-to-noise ratio required at the filter to satisfy this condition.

To retrieve data on the ground with 1 percent accuracy it is necessary only to detect which one of the banks of 100 contiguous filters is responding to the received signal tone. Noise in the filter bank will tend to obscure the true signal and give false indications as to which filter is responding at various times.

This situation is analogous to that of determining the bit error probability of a noncoherent FSK signal as a function of the signal-to-noise ratio at the system output. If a matched filter is used, the probability of error (i. e. , the probability that any single filter in the bank is selected when it should not have been, or is not selected when it should have been) is given by (Reference 2-2)

$$P_e = \frac{1}{2} e^{-E/2 N_o} \quad (2-5)$$

where

P_e = probability of error in a given filter

E = average signal energy in a burst

N_o = noise spectral density

An error rate of 10^{-3} will be considered. This means that above 99.9 percent of the data will be valid.

Therefore,

$$P_e = 10^{-3} = \frac{1}{2} e^{-\frac{E}{2N_0}}$$

$$\frac{E}{N_0} = 12.4 \text{ or } 10.9 \text{ db}$$

Actual tests on the ground system using live satellite data have shown that operation is within 3 to 6 db of that which could be obtained theoretically (Reference 2-3). Therefore, the value of E/N_0 will be increased by 6 db to obtain a more realistic result. Let

$$\frac{E}{N_0} = 16.9 \text{ db}$$

The value of N_0 has been previously determined as -199.2 dbw. Therefore,

$$E = 16.9 - 199.2 = -182.3 \text{ dbw}$$

E is the average signal energy in a burst and is the product of the usable signal power, P_s , and the duration of the burst, T .

$$E = P_s T \text{ or } P_s = \frac{E}{T} \quad (2-6)$$

The duration of each burst is 10 ms, or expressed in equivalent db, -20 db. Therefore,

$$P_s = -182.3 + 20 = -162.3 \text{ dbw}$$

The net loss was determined as 150.6 db. The power in the first sideband pair, P_{s1} , at the spacecraft transmitter is therefore given by

$$P_{s1} - 150.6 = -162.3$$

$$P_{s1} = -11.7 \text{ dbw}$$

or

$$P_{s1} = 68 \text{ mw}$$

The total transmitter power, P_T , is now readily determined from

$$P_{s1} = 2 P_T [J_1(\phi)]^2$$

The subcarrier oscillator in the spacecraft will phase modulate the carrier with a modulation index, ϕ , of about 1.2 radians. Therefore

$$P_T = \frac{P_{s1}}{2 [J_1(1.2)]^2} = \frac{68}{2(.4983)^2} = 137 \text{ mw}$$

An additional safety margin will be obtained if more transmitter power is used. Several transmitter powers and safety margins are tabulated below:

<u>Transmitter Power</u>	<u>Additional Safety Margin</u>
137 mw	0 db
250 mw	2.6 db
500 mw	5.6 db
1.0 watts	8.6 db
1.8 watts	11.2 db
2.0 watts	11.6 db

Telemetry Encoder

The block diagram in Figure 2-3 presents a means of implementing the Goddard PFM standard telemetry format specified in Reference 1-1. The encoder parameters are:

Data subcarrier frequency:	10 kcps, ± 50 percent deviation
Sync frequency (f_o):	4500 cps
Reference frequency (f_r):	one of the specified frequencies
Data rate:	50 data bursts per second
Number of data frames:	to be determined (16 maximum)

The channel rate oscillator is a 200-cps tuning fork oscillator which serves as a trigger for the channel selection counter. The channel selection counter consists of N flip-flops, where N is the smallest integer equal to or greater than $(6 + \log_2 n)$, and n is the number of data frames; there are 15 data channels per frame.

The reference frequency is obtained from either a tuning fork or crystal oscillator.

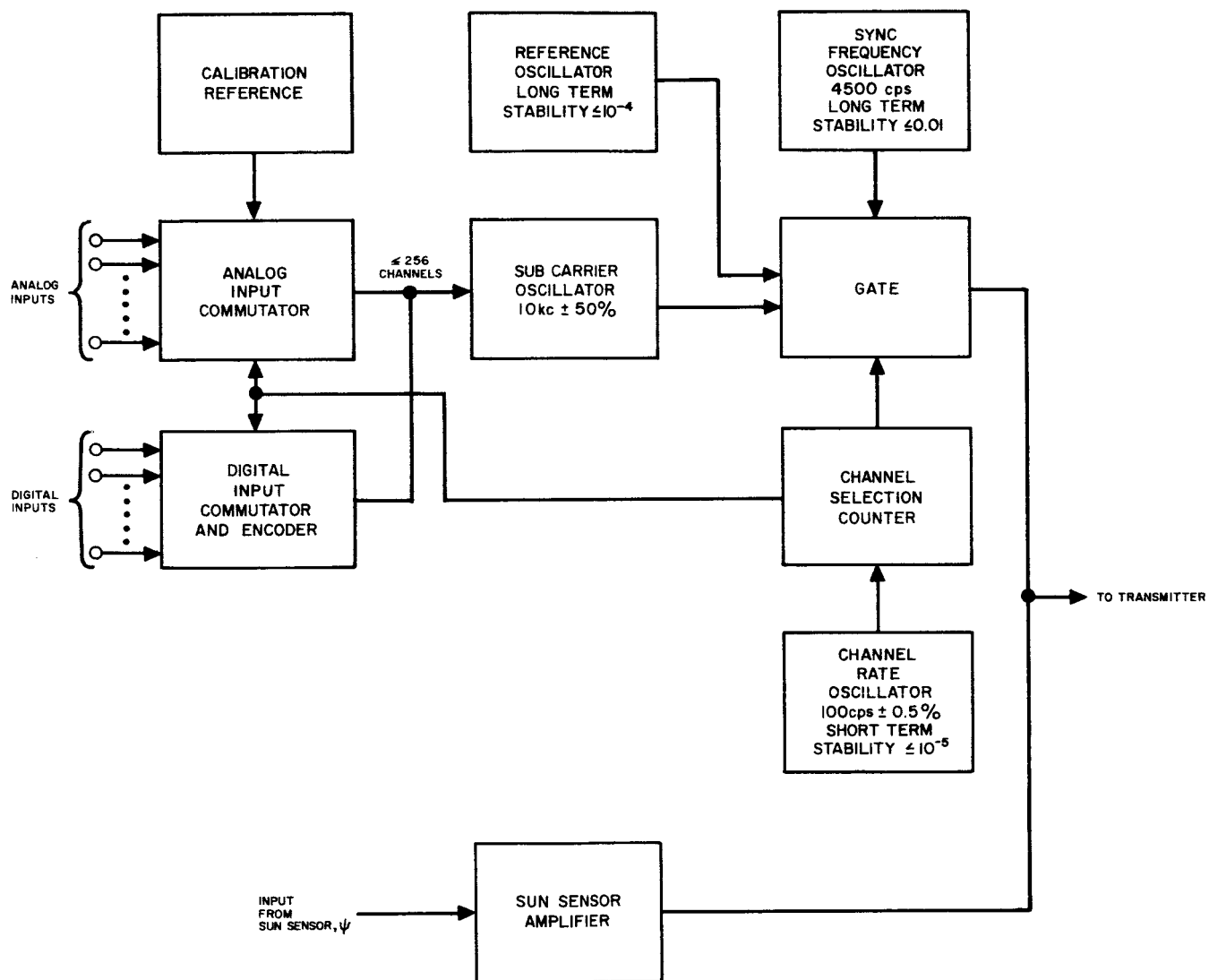


Figure 2-3. Syncom II Telemetry Encoder Goddard PFM Standard

The analog-input commutator selects the analog signal to be telemetered, as determined by the state of the channel selection counter, and switches the selected signal to the voltage-controlled oscillator. The digital-input commutator selects the digital binary signals to be telemetered, in groups of up to three bits at a time, and applies the selected signals to the digital-input encoder. The digital inputs to be selected are determined by the state of the channel selection counter. The digital input encoder converts the three (or less) digital signals into a corresponding voltage which may assume one of eight discrete levels corresponding to the eight possible states of the inputs. This voltage is then applied to the voltage controlled oscillator.

The stepped frame synchronization bursts are obtained by applying the outputs of the appropriate flip-flops of the channel selection counter to the digital input commutator.

The frame synchronization and reference frequencies are gated to the telemetry transmitter at the appropriate times as determined by the lesser significant bits of the channel selection counter.

The calibration reference provides an accurate known voltage which is applied as one of the analog inputs; ground potential is applied as another analog input, providing two-point calibration of the subcarrier oscillator.

The sun sensor pulses are amplified and linearly added to the PFM signal at the input to the telemetry transmitter.

Encoder Interface. Telemetry analog inputs are within the range 0 – +4 volts; telemetry digital inputs are $0 \leq V_0 \leq +0.5$ volts, $V_1 \geq +5.0$ volts, where V_0 and V_1 are the zero-state and one-state voltage levels, respectively.

The command decoder-telemetry encoder interface consists of three items of digital information:

Command register contents	7 bits
Phase angle of transponder antenna beam with respect to selected sun-sensor	9 bits
Sun-sensor selection	<u>2 bits</u>
	18 bits

The eighteen bits of information are telemetered on six data channels, three bits per channel. The digital input encoder converts each set of three bits into a voltage which assumes one of eight possible levels, corresponding to the configuration of the input bits.

COMMAND SUBSYSTEM

Command Decoder

A preliminary command decoder system design is shown in the block diagram in Figure 2-4. Description of operation of the decoder follows with reference made to the block diagram.

Primary Mode. The primary decoder mode operates from a NRZ format, frequency-shift-keyed digital wave train with inherent bit synchronization information. The information is contained in a sine wave whose alternate zero crossings are at the time center of the data bits. This sine wave amplitude modulates either the "zeros" tone or the "ones" tone, whichever is being transmitted.

Prior to command initiation the zeros tone with the bit synchronization wave is transmitted to the vehicle. This tone passes through tone filter #2 and hence to the audio detector. After a few cycles of the bit synchronization wave, the audio detector begins reproducing the bit synchronization sine wave. The sine wave is shaped into a square wave by the clock amplifier. The clock amplifier then provides bit shift signals to the command register, which, in primary mode, is connected as a shift register.

Following an interval sufficient to allow the buildup of clock pulses in the satellite, the command is transmitted. The order structure is:

bits 1-4
bits 5-11

word synchronization and address
data or command bits

Each of the redundant decoders has a separate digital address. When this address is detected, a latching enable switch is closed, which connects command power to the rest of the decoder. The command is then shifted into the command register. The block diagram is drawn assuming neither a one nor a zero tone is transmitted after the last data bit. Since the clock stops with neither frequency present, the shifting stops after the last data bit is received.

As in Syncom I, the commands are verified via telemetry prior to execution. After verification, execution is accomplished by transmitting a tone separate from either the ones or zeros tone. Execution commences with receipt of this tone and lasts as long as the tone is present. When the tone is removed, execution ceases and the trailing edge resets the enable switch, turning off decoder power. This technique permits execution in real time, a vital requirement for Syncom. This type of execution is not available in presently planned standard equipment, but from preliminary analysis of standard equipment specifications its inclusion could be accomplished by a simple adaptation to existing standard ground stations.

Backup Mode. The audio detector, which generates the bit shift clock in the satellite, is used to drive a biased detector with a large time constant. If the bit synchronization wave on either tone is left on for approximately 5 seconds, this biased detector changes state. This state change turns on the enable switch and changes the command register operation to count rather than shift. The commands can then be entered into the register by counting either the ones tone or the zeros tone as in Syncom I. Execution and verification are accomplished as in the primary mode.

Modified Requirements. Modifications of the command subsystem are being considered. These are concerned with the command capability to fire the gas jets. The current engineering model of the fire angle generator, a subassembly included in the phased-array antenna control electronic subsystem, has been designed to permit command initiation of a gas jet pulse at any angle (0.7 degrees resolution) relative to the spacecraft-to-sun direction. Simplification of the command subsystem results if the number of pulse initiation angles are reduced. Consideration is being given to permit initiation at only two angles, ± 90 degrees from the antenna beam direction. A modification is also planned which will permit either or both gas jets to be operated during a rotation of the spacecraft.

Decoder Interface. The decoder receives the following inputs:

- 1) NRZ format, frequency drift keyed digital wave train
- 2) Execution tone

The decoder provides three types of outputs:

- 1) For the control of power to other subsystems, the decoder provides normally open transistor switches which can be shorted to a negative voltage upon command
- 2) The decoder provides positive voltage logic signals for the firing of the control jets
- 3) The decoder provides positive voltage logic signals to the phased-array control electronics for positioning and adjusting the antenna beam

ORBIT ANALYSES AND SPACECRAFT DYNAMICS

Ascent Guidance Error Estimate

Recent revisions and corrections of the initial ascent guidance error estimates have resulted in the downgrading of the required velocity corrections from 370 (Reference 2-4) to approximately 250 fps (3σ). This value has been corroborated by the final Lockheed report (Reference 2-5).

Analytical Thrust-Misalignment-Model Check

An analytic model (Reference 2-6), to predict the effects of thrust misalignments of the third-stage (apogee) motor was checked against machine results given in Section 7 of Reference 2-6. The model predicts the subsequent attitude change α_1 of the angular momentum vector of the spinning spacecraft, the rotation γ_1 of the incremental velocity vector, and the induced nutation angle θ_1 . Using assumptions comparable with those of Reference 2-6 (e. g. impulsive tailoff), reasonable and conservative agreement is obtained except in the prediction of the postburnout nutation angle. The model predicts a nutation angle ranging from 0.83 to 4.8 degrees, while that indicated in Reference 2-6 is ~ 1.2 degrees. The larger model value is due to maximizing the magnitude of the model. A further check with machine results of Syncom I misalignment studies using linear tailoff, Reference 2-8, shows a more conservative value in nutation angle prediction (~ 2.6 degrees from the model versus 1.9 degrees from numerical computation). Model prediction of α_1 agrees with that of Reference 2-8 within ~ 0.1 degree.

This model may be used as a preliminary tool to determine thrust misalignment effects for various apogee motor design studies.

ELECTRICAL POWER SUBSYSTEM

General

Unregulated dc electrical power is supplied to the spacecraft bus from an array of *Non-P* silicon solar cells and hermetically sealed nickel cadmium batteries. (See Figure 2-5 for the electrical system schematic.)

The solar array forms the outer cylindrical surface of the spacecraft. For convenience of manufacturing and handling, the solar array has been divided into sixteen separate panels. Each panel is approximately 22 by 25 inches encompassing one-half the length of the spacecraft and 45 degrees of arc on the cylindrical surface.

Four 6-ampere-hour nickle-cadmium batteries are installed to provide electrical power for transient demands that exceed the solar panel output capability, and for electronic subsystem operation during the eclipse portions of the orbit.

Each battery is charged with a separate boost type of charging regulators.

Assumptions

- 1) Leakage current of subsystem post regulators
"ON" mode 3.5 ma
"OFF" mode negligible

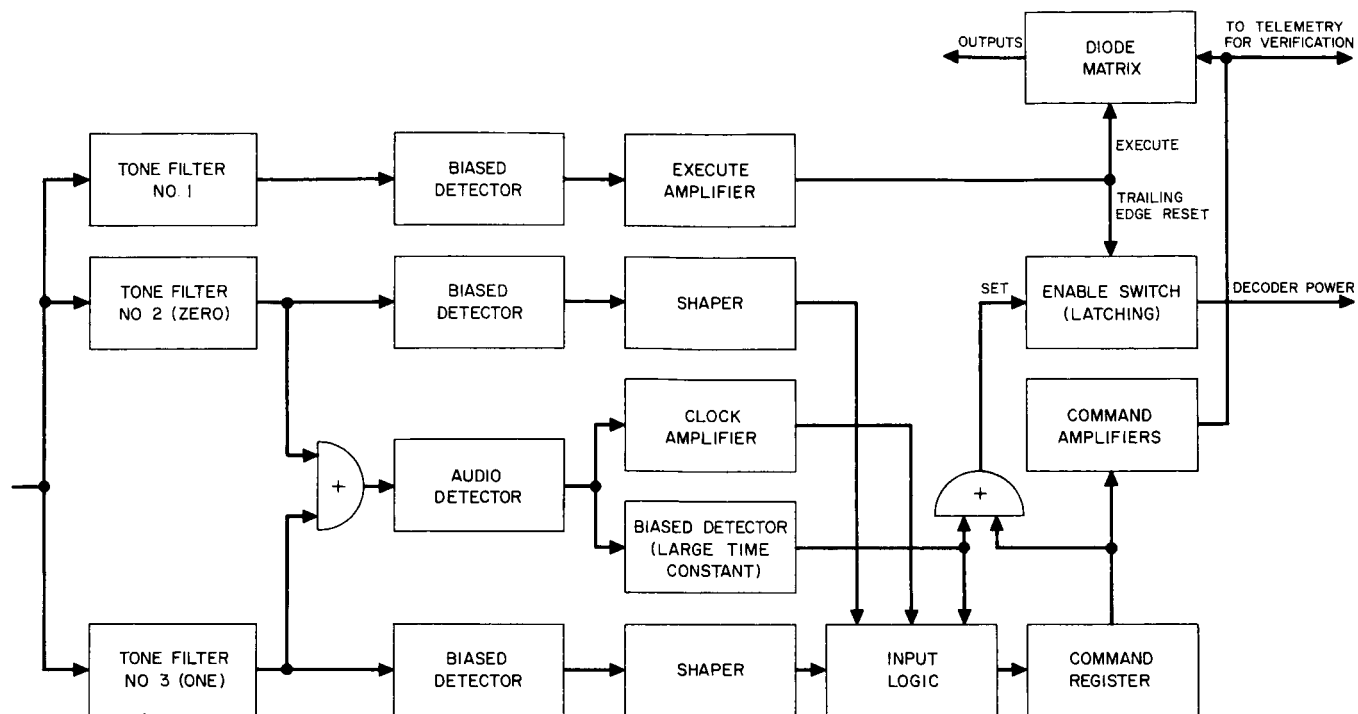


Figure 2-4. Syncom II Dual-Mode Command System

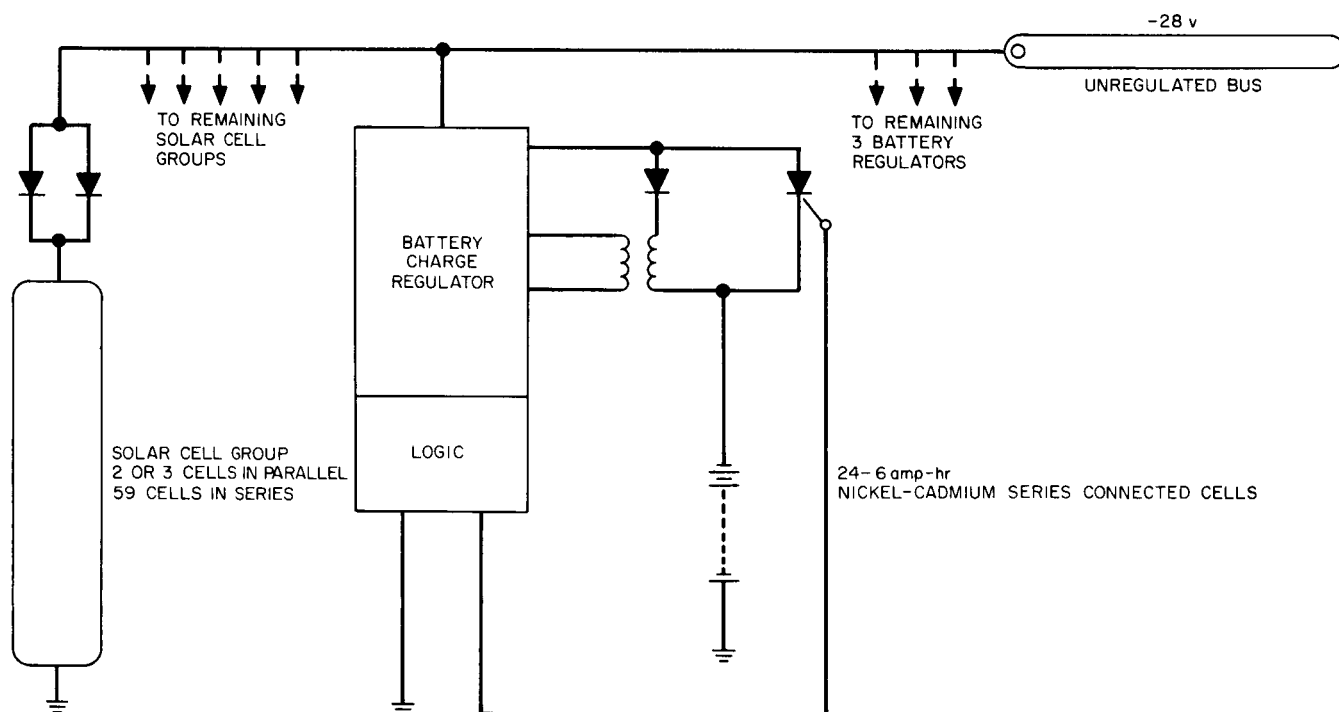


Figure 2-5. Electrical Power System Schematic

- 2) TWT efficiency — 30 percent dc-rf
TWT filament — 1.3 watts at 24 volts
TWT converter efficiency (high voltage and filament) — 90 percent
- 3) Battery charging rate and charging efficiency based on:
Two batteries capable of supplying complete spacecraft electrical load during eclipse
Available battery charging time 22.85 hours/orbit minimum
Battery discharging time 1.15 hours/orbit maximum
- 4) N-P low resistivity silicon solar cells employed with 9 percent efficiency minimum
- 5) Solar cell efficiency is based on the following conditions:
Air mass zero
.006 fused silica cover slides with ultra-violet filtering
Solar intensity 139 mw/cm²

Design Requirements

Solar panel temperature

normal incidence $B = 0^\circ$ $75^{+5}_{-10} \text{ }^\circ\text{F}$

oblique incidence $B = 25^\circ$ $60^{+5}_{-10} \text{ }^\circ\text{F}$

Battery temperature range 40 - 100^oF

Bus voltage > -26 volts at the input to the electronics systems post regulators.

Electrical Loads

Subsystem	Number Units/ Quadrant	Total Number Operating	ma/ Unit	Bus Load ma
Telemetry	2	1	245	245
Command receivers	2	8	27	216
Encoder	2	1	27	27
Antenna electronics	1	1	650	650
Communications receiver	2	4	75	300
TWT (4-watt)	2	3 During orbits with eclipse		2079
		4 During orbits without eclipse		2772
Battery charging	4	During orbits with eclipse		840
		4 During orbits without eclipse		300
Total bus load		During orbits with eclipse		5007
		During orbits without eclipse		5100

Solar Array

The solar array is composed of 22,240 1 by 2 centimeter n-p silicon solar cells connected in 128 series-parallel groups as shown in Figures 2-6 and 2-7. Each series-parallel group is connected to the spacecraft electrical bus with two blocking diodes in parallel. Series-parallel solar cell interconnections have been used to increase the electrical power system reliability.

Within the physical constraints of the spacecraft envelope, it is possible to install the solar cells on each panel in such a manner as to provide the desired 28-volt output with a single row of solar cells extending from the top to the bottom of each panel. Only by developing the entire bus voltage in this manner is it possible to provide sufficient paralleling of cells to enhance system reliability. Had it been necessary to use more than one row of cells to generate system bus voltage, paralleling of cells would have been impractical due to the resulting difference of individual cell illumination. Array electrical characteristics are shown in Figure 2-8.

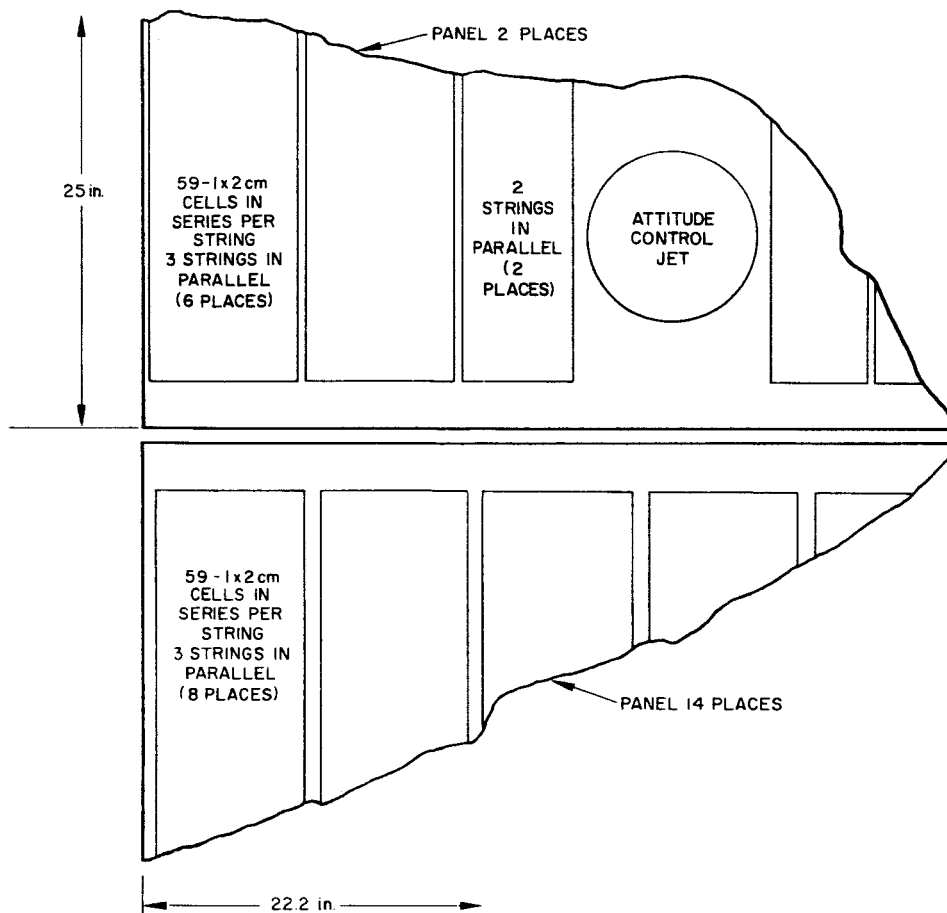


Figure 2-6. Solar Cell Panel Layout

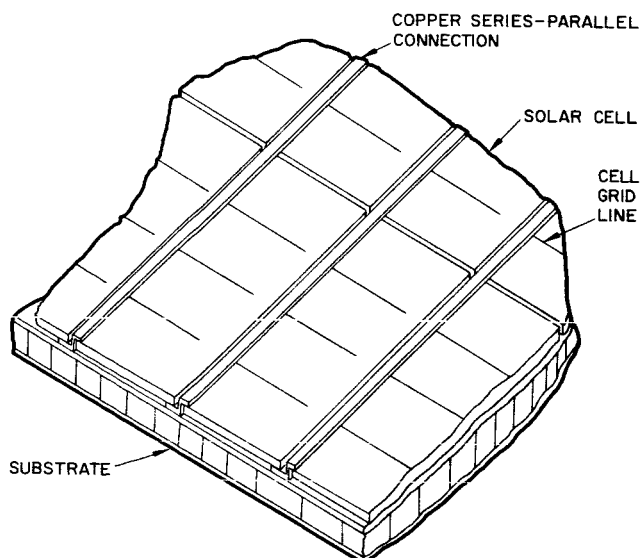


Figure 2-7. Solar Cell Mounting

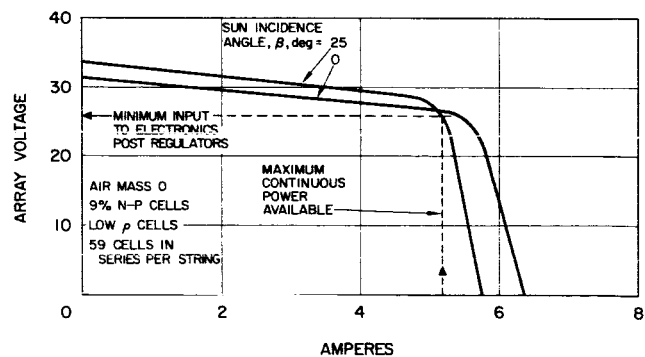


Figure 2-8. Solar Array Characteristics

N-p low resistivity cells are approximately 10 times more resistant to radiation damage than p-n type cells. Although high resistivity n-p cells have even greater radiation resistance than low resistivity types, their output voltage is significantly lower and their use would necessitate a 10 percent increase in spacecraft length to accomplish the desired series-paralleling connection of cells.

Batteries

Four 24-cell nickel cadmium batteries, each rated at 6 ampere-hours, are installed on the spacecraft. Twenty-three series-connected cells would be required to furnish the minimum bus voltage requirement (26 volts) during eclipse. One additional cell has been added to each battery to accommodate a single cell failure (shorted).

Rectangular cells with both the input and output terminals electrically insulated from the cell case will be used. Electrical insulation of the terminals from the cell case provides more adequate and uniform thermal conduction to the spacecraft structure. This results in more uniform battery cell temperatures, hence potentially increased system reliability. The use of cells with rectangular construction adds additional weight to the spacecraft. This additional weight is required to prevent deformation of the cell cases as a result of internal pressure buildup during sustained periods of overcharging.

The General Electric Company is investigating the addition of a sensory electrode, which senses oxygen pressure, for charging control. The signal produced can be easily used to provide battery charge limiting, thereby maintaining internal cell pressures low enough to permit usage of lighter weight spacecraft installation hardware. This sensory electrode development will be monitored by Hughes for possible application to the SYNCOM II program.

Battery Charge Regulator

Battery charge regulators used for Syncom II will be of a boost type as opposed to the loss type currently employed in the Syncom I design.

The 24-cell batteries used require charge battery terminal voltages in excess of 36 volts. Syncom I battery charge voltage is available only at times of reduction in electronics load demands. The use of a boost type of charging regulator permits battery charging continuously from the solar panel which at the same time minimizes the total number of series solar cells required. Use of a boost type regulator allows solar panel design to be based on the minimum voltage input to the electronics subsystems (-26 volts) rather than the high battery charge voltages required.

SYSTEM RELIABILITY STUDIES

Reliability Assurance

Reliability assurance requirements have been prepared for incorporation into the Syncom Mark II performance specifications. Detailed reliability requirements for each major subsystem have been defined to guide design, facilitate monitoring and development controls, and provide a basis for test planning and evaluation. The subsystem requirements are:

Communications. The mean-time-to-failure for at least one of four transponders providing successful communications shall be three years for the multiple access and two years for the frequency translation mode of operation. This minimum requirement for communications success is based upon continuous operation in either mode, i. e. , a 100-percent duty cycle, of all available communications transponders. The specified mean-time-to-failure includes the effect of boost and synchronization-orientation upon the orbital communications phase.

Tracking and Telemetry. The spacecraft shall provide an operable telemetry system during the orbital phase with a mean-time-to-failure of at least three years. The probability that spacecraft tracking will operate during the launch sequence shall be at least 0.99.

Reaction Control Subsystem. The probability that the spacecraft reaction control subsystem will survive the launch environment shall be at least 0.999. The probability that the reaction control subsystem will properly orient and maintain velocity corrections shall be at least 0.995 for one year with a minimum five-year lifetime.

higher
Power Supply Subsystem. The spacecraft power supply shall have a minimum lifetime of five years and shall be capable of continuous operation during eclipse. The probability that the power supply will operate continuously for three years shall be 0.95 as a design objective.

Apogee Motor Subsystem. The apogee motor shall be designed to provide a probability of success of 0.999 for its specified mission.

Structure. The structure shall provide basic support for the other subsystems of the spacecraft and for the attachment to the boost vehicle with a probability of success of 0.999 for five years.

Specific requirements for a time-phased reliability program have been also delineated for incorporation into the performance specification. These requirements encompass the following program elements. The program will be organized and scheduled to include designated milestones at which reliability will be objectively reviewed and reported. The program plan shall be directed toward reliability objectives established for each equipment and provide for direction of growth to meet ultimate objectives.

The reliability program plan will include organizational provisions for the scheduling and control with timely and adequate completion of such procedures as design reviews, requirement studies, failure mode analyses, indoctrination, evaluation tests, and failure analysis, reporting and corrective action. The reliability program plan will also include provisions for vendor selection and monitoring, a reliable parts program with adequate controls, parts lists, specifications, and periodic status reporting.

Additional reliability assurance tasks have included further analysis of the Syncom I reliability data to determine what changes in data acquisition procedures are desirable in the reporting system for Syncom Mark II.

Component acceptance and burn-in requirements are currently being determined. An investigation of procedures for control of parts through a bonded stores program, which is essential to the follow-on phase, has been initiated.

Design Analyses

The study initiated to enhance the reliability of the phased array antenna control circuits through improved parts application and applied redundancy at functional modes has continued. A detailed reliability analysis of the initial demonstrations model for this subsystem has yielded reliability estimates from which trade-off studies may be performed. It is expected that the phased array antenna control circuits design review scheduled for early January 1963, will result in further recommendations for special studies and circuit configuration trade-offs to improve the reliability of this subsystem. It may be noted that consistency of part types has been maintained throughout the subsystem and the number of different part types will be kept to a minimum in subsequent circuit modifications.

The reliability program during this reporting period has also included reliability discussions with cognizant design engineers and analyses of several power supply configurations. This effort has been directed toward the optimization of the solar electric panel layout for maximum power output, ease of fabrication through simplification of interconnections, enhancement of reliability through parallel redundancy of strings and minimum cost. Promising power supply configurations in addition to that selected will be given further detailed analysis, including both n-p and p-n solar cell types for the panel, and examined for high reliability using the best available failure data and analysis techniques.

TEST EQUIPMENT

Specification for the Advanced Syncom ground support equipment has been prepared for inclusion in the system performance requirements specification. This specification includes requirements for general design functional test and support, electrical and physical design, reliability control,

and service conditions. A preliminary description of the planned system test equipment has also been prepared. Commercial test equipment required for the system test equipment has been listed and special panels have been defined in general terms.

Testing of Syncom II Transponder Multiple Access Mode

This section presents preliminary requirements for checkout of the multiple access mode of the communication transponders. Included are descriptions of system tests, a preliminary equipment list, and a test equipment block diagram.

Test Concept. The tests formulated provide checkout with access to the spacecraft through the transmitting and receiving antennas only. The tests studied to date provide an indication of the operational status of the transponder. Wherever practical, ground station equipment is specified for test equipment. Thus, the single sideband exciter used in the test equipment will be identical to the ground communication station equipment. Thus unique special-purpose test equipment requirements are minimized and spacecraft-ground station compatibility is verified.

System Tests. It is anticipated that the following tests will be required to verify the operational capability of the multiple access mode of the Syncom II transponder. Except where specifically stated otherwise, access to the spacecraft will be limited to the transmitting and receiving antennas as indicated in Section II.

- 1) Receiver Sensitivity and Dynamic Range. The sensitivity of the multiple access receiver can be checked by monitoring the spacecraft response to a low level SSB signal.

The spacecraft RF signal can be monitored directly on a spectrum analyzer, and/or the demodulated signal can be monitored on an oscilloscope. The readability of a voice-modulated transponded signal may also be checked.

The dynamic range of the multiple access mode receiver can be checked by monitoring the spacecraft response to a high level SSB signal. Again, the spacecraft RF signal can be monitored directly on a spectrum analyzer, and/or the demodulated signal can be monitored on an oscilloscope. In either case, there should be no evidence of receiver saturation for input signal levels of less than a given magnitude.

The low level and high level SSB test signals will be provided by the test equipment from a variable power output generator.

2) Transponder Bandwidth. The bandwidth of the multiple access transponder can be checked by monitoring the spacecraft response to a wideband (5-mc) SSB signal on a spectrum analyzer. The wideband SSB signal will be provided by the test equipment, and two kinds of wideband signals could be generated depending upon the sideband information desired:

- a) The first signal would have sidebands corresponding to three or more channels. As a minimum requirement, sidebands should be generated at the extreme ends and middle of the 5-mc as during actual ground station operation. A more complete check would be obtained with 600 sidebands uniformly spaced throughout the entire 5-mc band. The feasibility of generating many sidebands will depend upon the manner in which the channel and group carriers are derived in the multiplexing equipment.
- b) A second type of wideband signal would be frequency-swept across the entire 5-mc band. Such a signal could be obtained by driving the microwave modulator with a frequency swept signal. This alternative has the disadvantage of introducing a requirement for a sweeping generator.

3) Phase Modulation Index. The modulation index of the phase-modulated spacecraft return signal will be checked while providing an SSB input signal having specified modulation and frequency characteristics. The SSB signal shall be specified so as to check the phase modulator under the "worst case" conditions. A spectrum analyzer should be suitable for monitoring the modulation index although it may also be monitored at the demodulator output.

4) Power Output. Transponder output power will be measured with an RF power meter to verify that the transponder is delivering rated output power. The power spectrum can also be checked with a spectrum analyzer at this time.

5) Frequency Stability. Frequency stability of the multiple access transponder can be checked by monitoring the receiver master oscillator and transmitter master oscillator and comparing to a very stable frequency source. Access to the spacecraft must be provided.

6) Intermodulation Distortion. Intermodulation distortion may be checked by two tests:

- a) Wideband Noise Modulation - The test equipment will generate an SSB signal which has been modulated by wide-band noise containing a narrow noiseless window. When the spacecraft

retransmits this test signal, intermodulation components will appear in the noiseless window. The noiseless window will be positioned at various frequencies across the 5-mc band. A spectrum analyzer will be used to determine the intermodulation frequency components occurring at each position of the window. The demodulated output present in the audio channel corresponding to the noiseless window can also be monitored for intermodulation components.

- b) Audio Modulation - The test equipment will generate an SSB signal which has been modulated with two audio frequency sine waves. The sidebands produced by the two audio frequencies should differ by at least 4 kc but less than 8 kc to simulate clear tones located in adjacent audio channels. A spectrum analyzer will be used to check the spacecraft return signal for intermodulation components.

Note that both tests give an indication of distortion due to intermodulation between two or more different audio channels. Intermodulation distortion due to two frequencies in the same audio channel could also be checked simply by choosing the two frequencies such that the resulting sidebands differed by less than 4 kc.

- 7) Noise Figure. Reference Z-9 shows that the major component of transponder noise will be contributed by the SSB receiver. Therefore, a noise figure check of the SSB receiver would be effectively a noise check of the transponder. Such a test would require a noise generator, power meter, and a test point at the output of the IF amplifier.

Since receiver sensitivity or transponder functional performance will be checked on a system basis, it may not be necessary to measure noise figure except in unit tests.

- 8) Image Response. Image response can be checked by observing the transponder output spectrum resulting from an SSB input signal corresponding to the image frequency of the transponder. The results of this test could be expressed in terms of an image rejection ratio which must exceed some specified minimum value.

Block Diagram. The test equipment block diagram in Figure 2-9 shows the equipment necessary to check out one multiple access transponder of the Syncom II spacecraft. Some duplication of test equipment is required to check out the remaining three transponders.

Assuming that for test, it is not necessary to operate two or more transponders simultaneously, only the following equipment need be duplicated for each transponder:

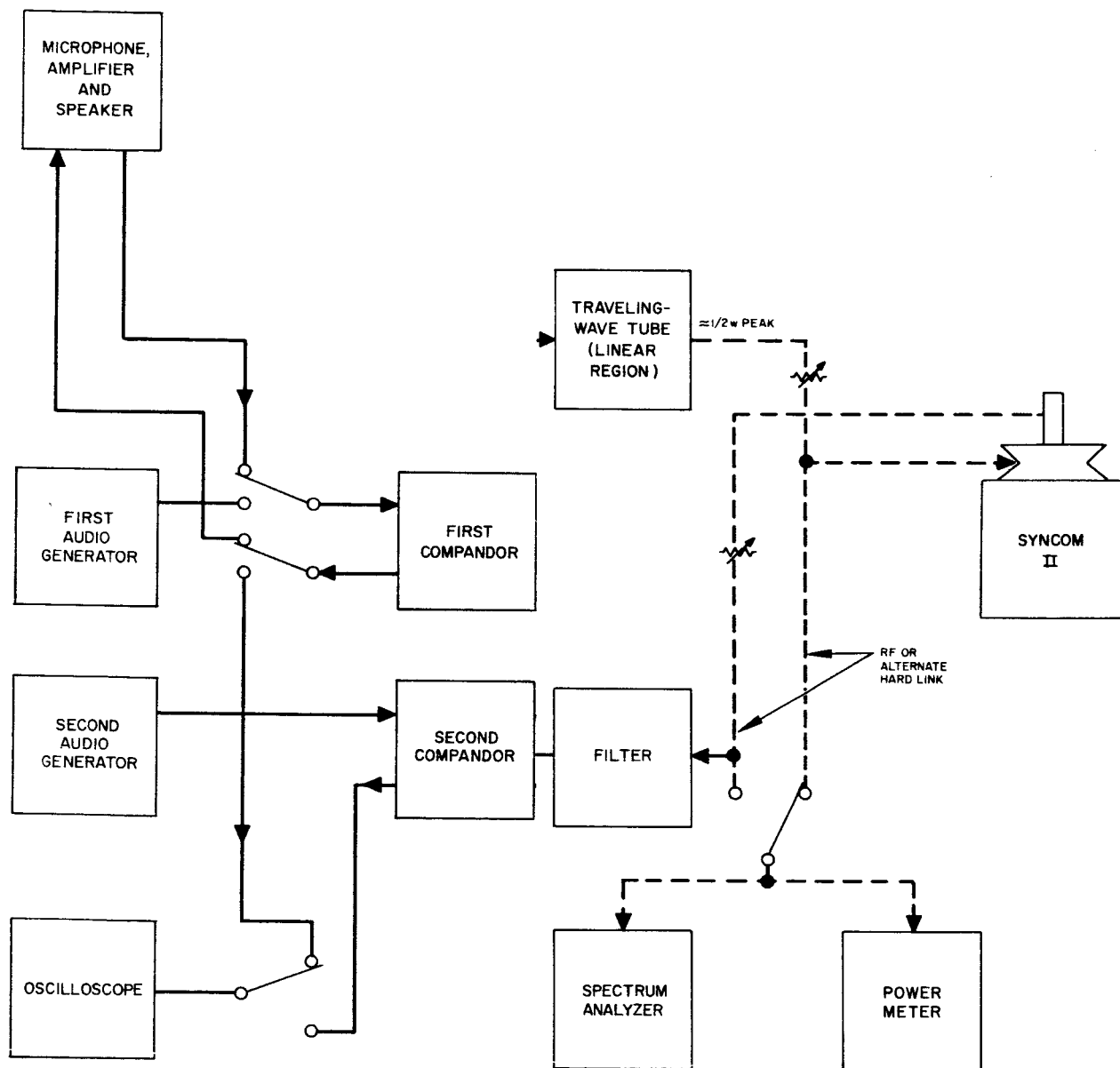
- a) Microwave drive to balanced mixer
- b) Microwave sideband filter
- c) Microwave filter of PM receiver
- d) Local oscillator signal of PM receiver

If it is desirable to test simultaneously more than one transponder, the entire block diagram must be duplicated with the exception of the following equipment:

- a) First and second audio generators
- b) Channel modulator and demodulator (it is assumed this equipment has a 12-channel capacity)
- c) Group modulator and demodulator (it is assumed this equipment has a 5-group capacity)
- d) Noise generator and narrow band reject filter
- e) Power meter, oscilloscope, and spectrum analyzer

Test Equipment Required. Test equipment expected to be required for testing the multiple access mode of the transponder is listed as follows:

<u>System Test</u>	<u>Test Equipment Required</u>
Receiver sensitivity and dynamic range	SSB generator } See note below PM receiver } Spectrum analyzer/oscilloscope Power meter
Transponder bandwidth	SSB generator Spectrum analyzer (optional equipment - sweeping generator)
Phase modulation index	SSB generator Spectrum analyzer
Power output	SSB generator Power meter Spectrum analyzer



INPUTS AND OUTPUTS OF CHANNEL AND GROUP MODULATORS AND DEMODULATORS ARE PATCHED AS REQUIRED.

Figure 2-9. Block Diagram of Test Mode of Syncom II

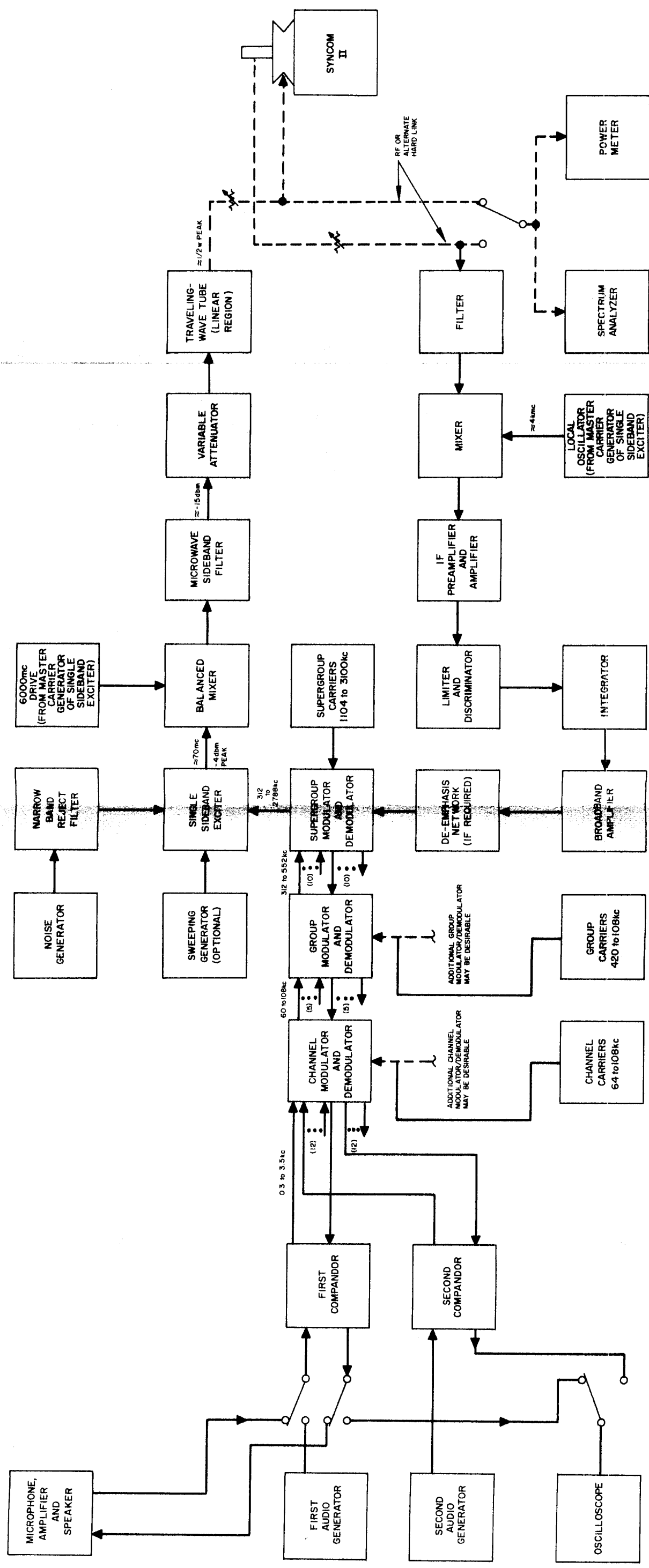


Figure 2-9. Block Diagram of Test Equipment for Multiple-Access Mode of Syncom II Transponder

<u>System Test</u>	<u>Test Equipment Required</u>
Frequency stability	Stable reference frequency source
Intermodulation distortion	Noise generator (VHF range) Narrow band reject filter SSB generator PM receiver Spectrum analyzer
Noise figure	Noise generator (6 KMC range) Power meter
Image response	SSB generator Spectrum analyzer

NOTE: The SSB generator is composed of the following pieces of equipment:

- Audio generators (2 required)
- Microphone, power amplifier, and loudspeaker
- Volume compressor (part of compander - 2 required)
- Channel modulator and carrier generators
- Group modulator and carrier generators
- SSB exciter
- Microwave balanced mixer
- Microwave carrier generator (6 KMC)
- Sideband filter
- Variable attenuator
- Linear TWT
- Adaptor for providing hard line connection to spacecraft receiving antenna (biconical horn)

The PM receiver is composed of the following pieces of equipment:

- Adaptor for providing hard line connection to spacecraft transmitting antenna (phased array)
- Local oscillator
- 4 KMC filter
- Microwave mixer
- IF preamplifier and amplifier
- Limiter and discriminator
- Integrator
- Broadband amplifier
- Deemphasis network (if required)
- Group demodulator and carrier generator
- Channel demodulator and carrier generator
- Volume expander (part of companders - 2 required)

REFERENCES

- Reference 2-1 "Preliminary Standard for Spacecraft Pulse Frequency Modulation," NASA-Goddard Space Flight Center, 4 September 1962.
- Reference 2-2 A. B. Glenn, "Companion of PSK vs FSK and PSK-AM vs FSK-AM Binary Coded Transmission Systems," IRE Transactions on Commercial Systems, p. 92, June 1960.
- Reference 2-3 C. J. Creveling, et al, "Automatic Data Processing" IRE Transactions on SET, p. 128, June 1962.
- Reference 2-4 Initial Project Development Plan, Volume 1, Technical Plan, Hughes Aircraft Company SSD 2380R, NASA Contract 5-2797, 15 August 1962.
- Reference 2-5 "Final Report, Syncom Booster Feasibility Study," LMSC-A057612, 30 September 1962 (Confidential).
- Reference 2-6 D. D. Williams, "Dynamic Analysis and Design of the Synchronous Communication Satellite," Hughes Aircraft Company TM 649, May 1960.
- Reference 2-7 A. J. Iorillo, "Rotation of Syncom Angular Momentum Vector Due to Apogee Motor Malalignment," Hughes Aircraft Company IDC 2241.5/85.
- Reference 2-8 "Single-sideband to Phase Modulation Multiple Access Communication System Analysis," Hughes Aircraft Company TM 721.

3. ADVANCED TECHNOLOGICAL DEVELOPMENT

DUAL MODE TRANSPONDER

Circuits Common to Frequency Translation and Multiple-Access Transponder

X32 Multiplier

Additional X32 multipliers have been fabricated, completing all circuit application requirements. Three of these units have been checked out and meet system requirements. Fabrication of the bias supplies for these units will be initiated during the next report period.

X3 Multiplier

A developmental breadboard of the X3 multiplier (Figure 3-1) was completed during the report period. The initial breadboard employed tunable sections throughout. Based on the measurements made on this model, fabrication of the additional units required has been initiated, using fixed-length sections.


X2 Multiplier

Fabrication of the final configuration doubler has been initiated based on the testing accomplished on the tunable breadboard previously reported.

Circuits for FM Frequency Translation Transponder

IF/Limiter (25 mc)

A three-stage breadboard has been completed which exhibits excellent linearity over the 25-mc bandwidth. An additional three-stage section is being constructed to test reproducibility of this circuit. The final configuration IF amplifier will employ six stages to obtain the required gain.



Dual Filter Hybrid (2112 mc)

Delivery of three filters for the dual filter hybrid (Figure 3-2) has been completed. One filter failed to pass the Hughes acceptance tests and was returned to the vendor.

Specifications are as follows:

Center frequency (f_o)	2112 mc
Insertion loss (f_o)	1.25 db maximum
VSWR (f_o)	1.20:1 maximum
Rejection ($f_o \pm 40$ mc)	40.0 db minimum
Hybrid output ratio	6.0 db \pm 0.5 db
Hybrid directivity (f_o)	20.0 db minimum
Isolation between filters ($f_o \pm 40$ mc)	90.0 db minimum
Weight	8 ounces maximum

Dual Single-Sideband Filter - Diplexer (4080-4170 mc)

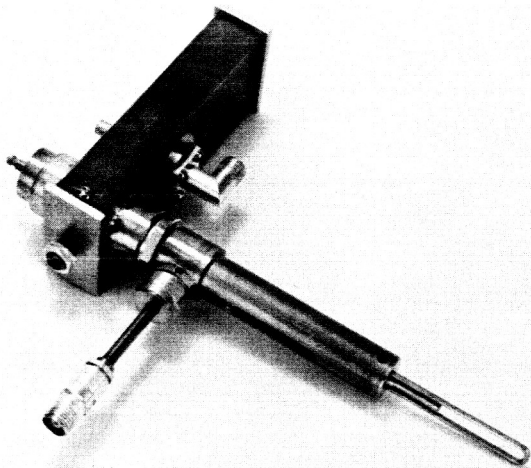
One of three of the dual single-sideband filter-diplexers on order has been delivered, and checkout testing is under way (Figure 3-3). Delivery of the remaining units is expected during the next report period.

Specifications are as follows:

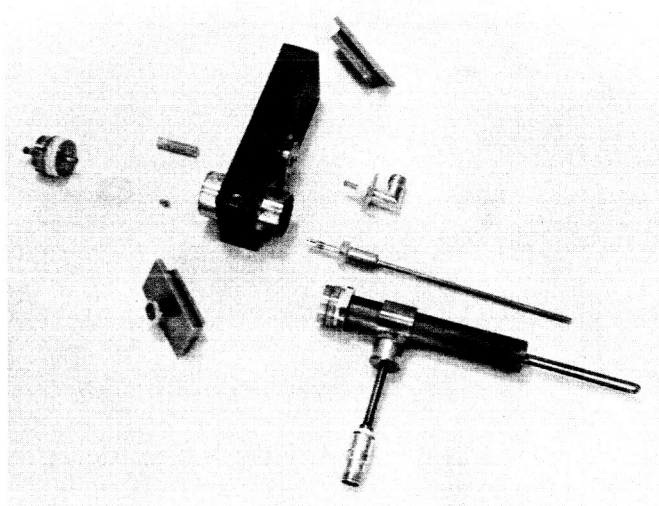
Frequency (f_{1o})	4080 mc
Insertion loss	1.0 db maximum
Bandwidth at 1.2 VSWR	25 mc minimum
Rejection at 4170 mc	25 db minimum
Frequency (f_{2o})	4170 mc
Insertion loss	1.0 db maximum
Bandwidth at 1.2 VSWR	25 mc minimum
Rejection at 4080 mc	25 db minimum
Weight	6.5 ounces maximum

High Level Mixer

Modification of Syncom I mixer mounts for compatibility with Syncom II frequencies is under way. A branch-line hybrid is being developed for use in this mixer.



a) Assembled



b) Exploded

Figure 3-1. Breadboard X3 Multiplier

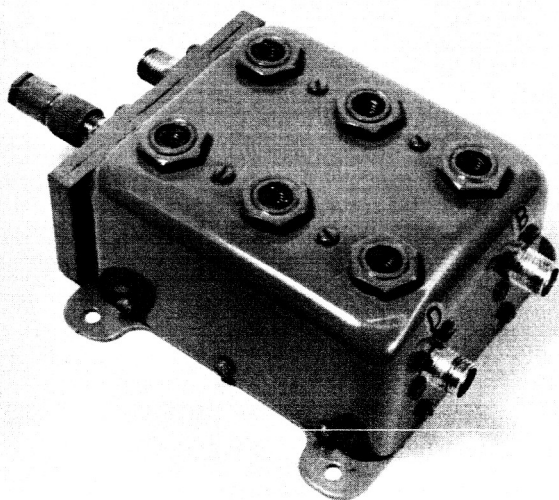


Figure 3-2. 2112 mc Dual
Filter Hybrid

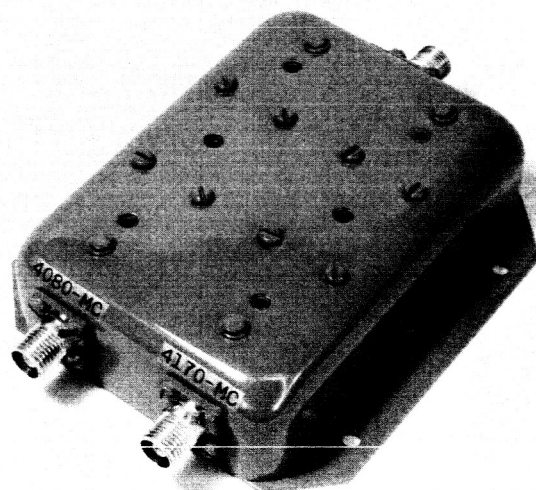


Figure 3-3. 4080-4170 mc Dual Single
Sideband Filter Diplexer

14 db coupler (4224 mc)

Fabrication and checkout of the necessary couplers has been completed (Figure 3-4).

Isolator (2112 mc)

Assembly of one of the isolators has been completed. Tests on the assembled isolator indicate satisfactory performance. Assembly of the remaining isolators is in progress.

Circuits for Multiple-Access Transponder

Isolators (2085 and 2119 mc)

Assembly of one of the 2119 mc isolators has been completed. Assembly of the remaining isolators and testing for circuit performance adequacy will be completed during the next report period.

Single-Sideband Filter (2085 mc)

Delivery of three single-sideband filters (Figure 3-5) has been completed. The filters have been tested and meet the following specifications:

Resonant frequency	2085 mc
Bandwidth	
1.20:1 VSWR	16 mc minimum
25.0 db	110 mc minimum
Insertion loss	0.75 db maximum
VSWR	1.20 : 1 maximum
Weight	2.5 ounces maximum

Filter (2119 mc)

Delivery of three 2119-mc filters has been completed. The filters have been tested and meet the following specifications:

Resonant frequency	2119 mc
Bandwidth	
1.20 : 1 VSWR	6.0 mc minimum
50.0 db	132 mc maximum
Insertion loss	1.25 db maximum
VSWR	1.20 : 1 maximum
Weight	2.5 ounces maximum

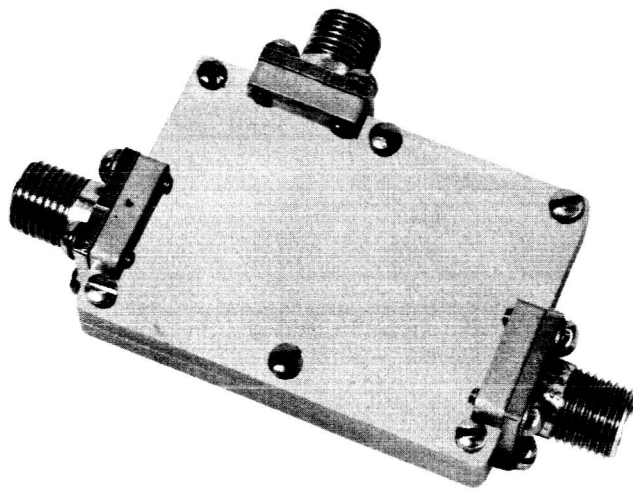
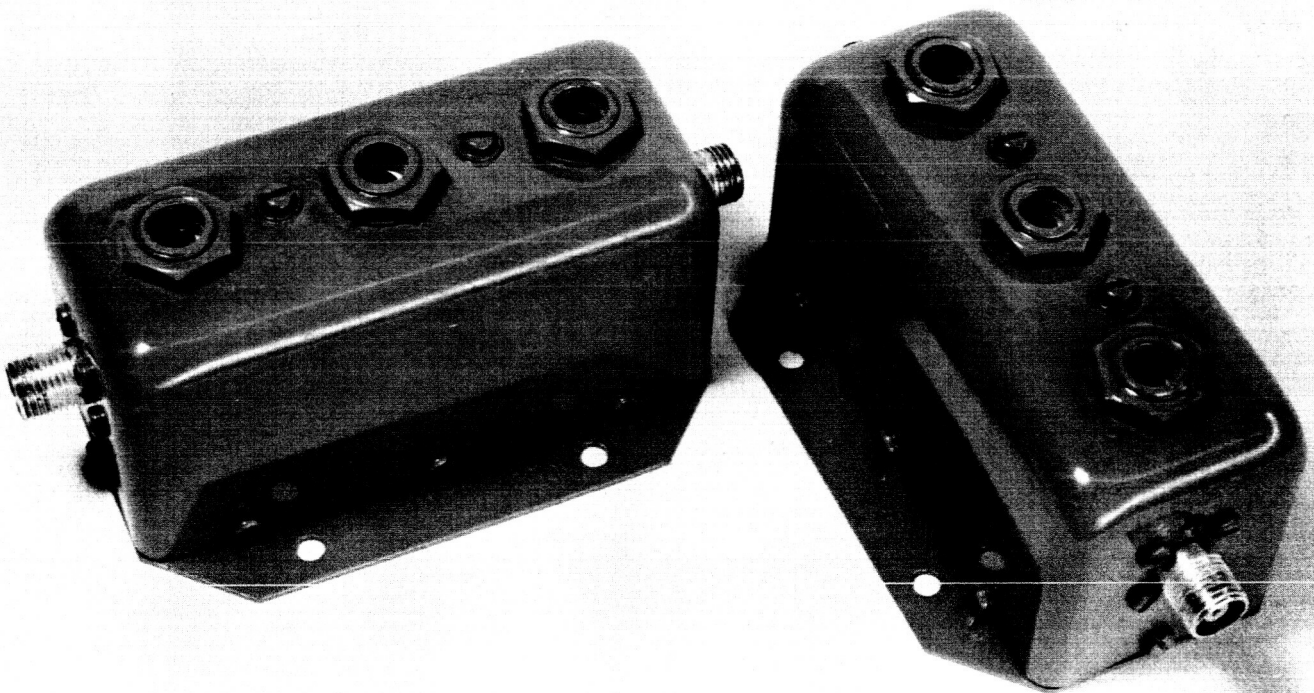


Figure 3-4. 14-db Coupler



a) 2085 mc

b) 2119 mc

Figure 3-5. Single-Sideband Filters

Dual Mode Transponder Test and Demonstration Panel

The test and demonstration equipment will perform the following evaluations on the transponder:

- 1) Receiver sensitivity
- 2) Transmitter power output
- 3) Baseband frequency response characteristic
- 4) Intermodulation distortion
- 5) Two-way voice demonstration

These tests will be accomplished as shown in Figure 3-6. Baseband signals in the range of 0.1 to 5.0 mc are converted to double-sideband suppressed carrier signals in the first balanced modulator (shown at the upper left in Figure 3-6). A bandpass filter rejects the lower sideband, leaving single-sideband suppressed carrier signals in the 32.58 to 37.58 mc range. A second balanced modulator converts this signal to 6390 mc. The power level at this point is measured on a microwave power meter. This signal is then attenuated and fed to the spacecraft transponder. The permissible degree of attenuation at this point will give a measurement of receiver sensitivity.

The transmitted signal from the transponder is sent through an attenuator and directional coupler to a power meter to measure output power. A signal out of the directional coupler is also sent to the receiver. The receiver detects the phase-modulated transponder signal and reproduces the baseband signals at its output.

Baseband frequency error due to transmit oscillator error and transponder local oscillator error is corrected by an automatic frequency control circuit. This circuit compares the frequency of a 284 kc signal inserted at the baseband input with that of the same 284 kc signal at the receiver output. A dc correction signal is produced which is proportional to the frequency difference of these two signals. This dc error correction voltage is fed to a varactor diode circuit which pulls the crystal oscillator frequency, thereby correcting errors in the system.

The baseband frequency response characteristic is tested by a generator having a crystal-controlled signal every 100 kc over the range from 0.1 to 5.5 mc. This signal is fed to the baseband input of the test transmitter. The detected output of the spacecraft transponder is measured over the baseband range to determine its characteristic.

Intermodulation distortion is measured by means of a Marconi Instrument Type OA1294B white noise test set. This equipment has been received and checked out.

A demonstration of two-way voice communication is made by use of two single-sideband transmitter-receiver units. These units generate a receive single-sideband signal in the baseband region.

Design of these items is essentially complete. Delivery of most long-lead-time items is scheduled in the first half of January 1963.

Problem Areas

Sideband Filter - 32 to 37 mc. This item will require several weeks of development. The major problem area is the requirement for fast rolloff near the carrier, while maintaining a high percentage bandwidth. Since this requirement precludes a crystal lattice configuration, it will be accomplished with L-C circuits.

Receiver Discriminator - 70 mc. A detector for phase-modulated signals remains to be developed. A discriminator having linear response over a 25 mc span centered on 70 mc is required. Several satisfactory designs are being investigated. Procurement of this item from Lenkurt Electric Co., Inc., has been initiated, but delivery schedules have not been finalized.

TRAVELING-WAVE TUBE

The effort during this period was divided into two areas: to build and evaluate tubes for a power output of 2.5 watts and to modify the present 2.5-watt design to achieve an output power of 4.0 watts. The inconsistency of the data obtained and reported last month after tube No. 384H-7 was packaged was traced to a mechanical fault in the output match. This was corrected and the tube was delivered on 17 December for laboratory use.

At a frequency of 4000 mc, this tube had the following performance characteristics:

Output power	2.5 watts
Gain	24 db
Efficiency	25.3 percent

Two tubes utilizing the longer helix were assembled to the prepackaging stage; however, only one (384H-8) could be tested because of a faulty vac-ion pump supply used on the other tube. An attempt is under way to repair or change the supply to avoid losing the tube. Although evaluation of tube 384H-8 is not yet completed, early data indicates that the increase in helix length raised the gain to 35 db as planned.

The helix pitch has now been changed to achieve 4.0 watts power output at 4000 mc. Construction of tubes utilizing this change is being expedited to obtain an early evaluation of the design.

Tube 384H-8, because of good focusing characteristics at high beam perveance, is expected to meet all the requirements of the new specifications. A more complete evaluation of this tube is being made.

PHASED ARRAY TRANSMITTING ANTENNA

Array Development

The vertically polarized antennas were assembled with the phase shifters and power splitter, and laboratory tests of the assembly were initiated. A check was made of the omnidirectional pattern (without current in the phase shifter field coils); although difficult to accomplish in a closed laboratory, it indicated some large fluctuations. The antenna was disassembled and the phase length of each of the phase shifters and cables was measured and matched up for reassembly to give a minimum variation. The omnidirectional pattern measurements were then repeated, with more satisfactory results.

Some preliminary tests of the directional pattern were made by putting a dc voltage on the field coils and mechanically rotating the coils to give the proper phase shifts. It was noted that the gain varied very little with changes in the applied voltage and that the best value was approximately 20 volts.

RF Circuits

Phase Shifters

All eight phase shifters were assembled and aligned. The output couplers were positioned to give in-phase RF outputs with no current in the coil. The coils were indexed so that, with dc voltage applied, they provided in-phase outputs. The phase lengths and losses of all eight were checked. In one case, parts from two phase shifters were interchanged to afford better performance. The isolation between output parts for these breadboard couplers was measured at about 15 db. (This could be potentially troublesome since reflected or mutually coupled power at one antenna can then be coupled to another and affect the pattern.) The stripline couplers of the engineering model coupler design should eliminate this problem.

An additional problem encountered was that some of the ferrites were apparently magnetized both laterally and longitudinally. After being de-gaussed in an alternating field, they were found to operate satisfactorily. With the normal current used in the field coil, the ferrites do not become magnetized.

Stripline System

A simplified diagram of the stripline output system being designed for the engineering model antenna is shown in Figure 3-7, for one coupler and a pair of antennas. The unit includes a four-probe waveguide-to-stripline

coupler, two baluns for coupling opposite probes out of phase, two matching sections, and a 90-degree hybrid. The antennas will connect to the stripline by TM connectors. Due to the geometry involved, there are a number of points where two striplines must cross over. The circuits will therefore be made in two planes with vertical transitions connecting them where necessary. To facilitate early testing of this system, an interim model is being fabricated (Figure 3-8). The four-probe coupler and hybrid-balun are constructed as separate units. Four equal lengths of coax will be used to connect them, and two other coaxes will connect to the antenna.

Control Electronics

Circuit and subsystem descriptions were prepared and a reliability estimate made during the report period for inclusion in a design inventory covering the phased array control electronics. The design review is scheduled for 3 January 1963. Studies are continuing on methods of reducing the quantity and varieties of components to increase reliability.

Layout of all circuit cards has been completed. At the end of the report period, digital card assembly was 75 percent complete and analog card assembly was 50 percent complete. Figure 3-9 shows cards being tested. Card checkout equipment will be completed early in January.

Waveform Generators and Amplifiers

The circuits required for generating excitation to the electromagnetic field coils of the ferrite phase shifters consist of an adding network followed by 16 waveform generators and power amplifiers. One channel of this circuit is shown in Figure 3-10. The output currents of the 16 power amplifiers are delivered to the 16 field coils of the eight ferrite phase shifters associated with the antenna array.

Input and Output Requirements. The adding network requires three input signal voltages as follows:

$$e_a = A \sin 2 \pi f t$$

$$e_b = A \cos 2 \pi f t$$

$$e_c = -A \sin 2 \pi f t$$

where the amplitude A is approximately 4.5 volts and the frequency f is approximately 1.67 cps.

The adding network is required to produce eight sine-wave output voltages, as follows:

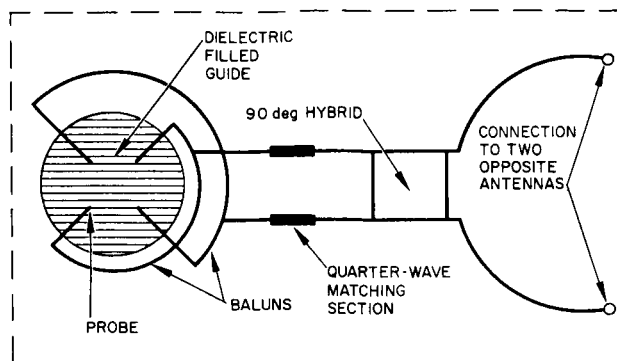


Figure 3-7. Stripline Output Coupler for Phased-Array Phase Shifter

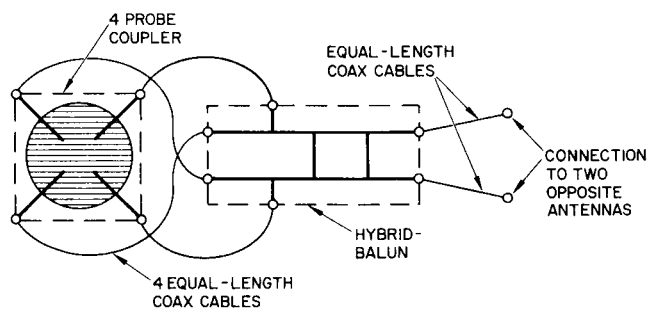
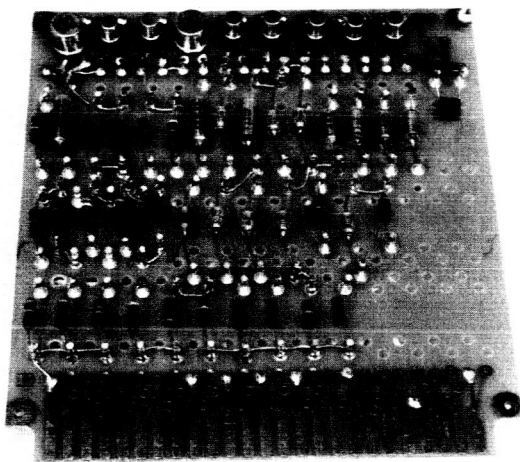
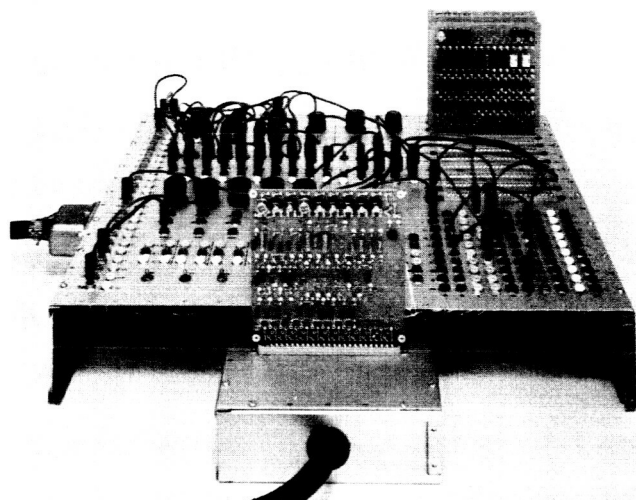


Figure 3-8. Interim Model of Stripline Coupler



a) Typical Card



b) Tester



c) Cards Under Test

Figure 3-9. Antenna Control Electronics

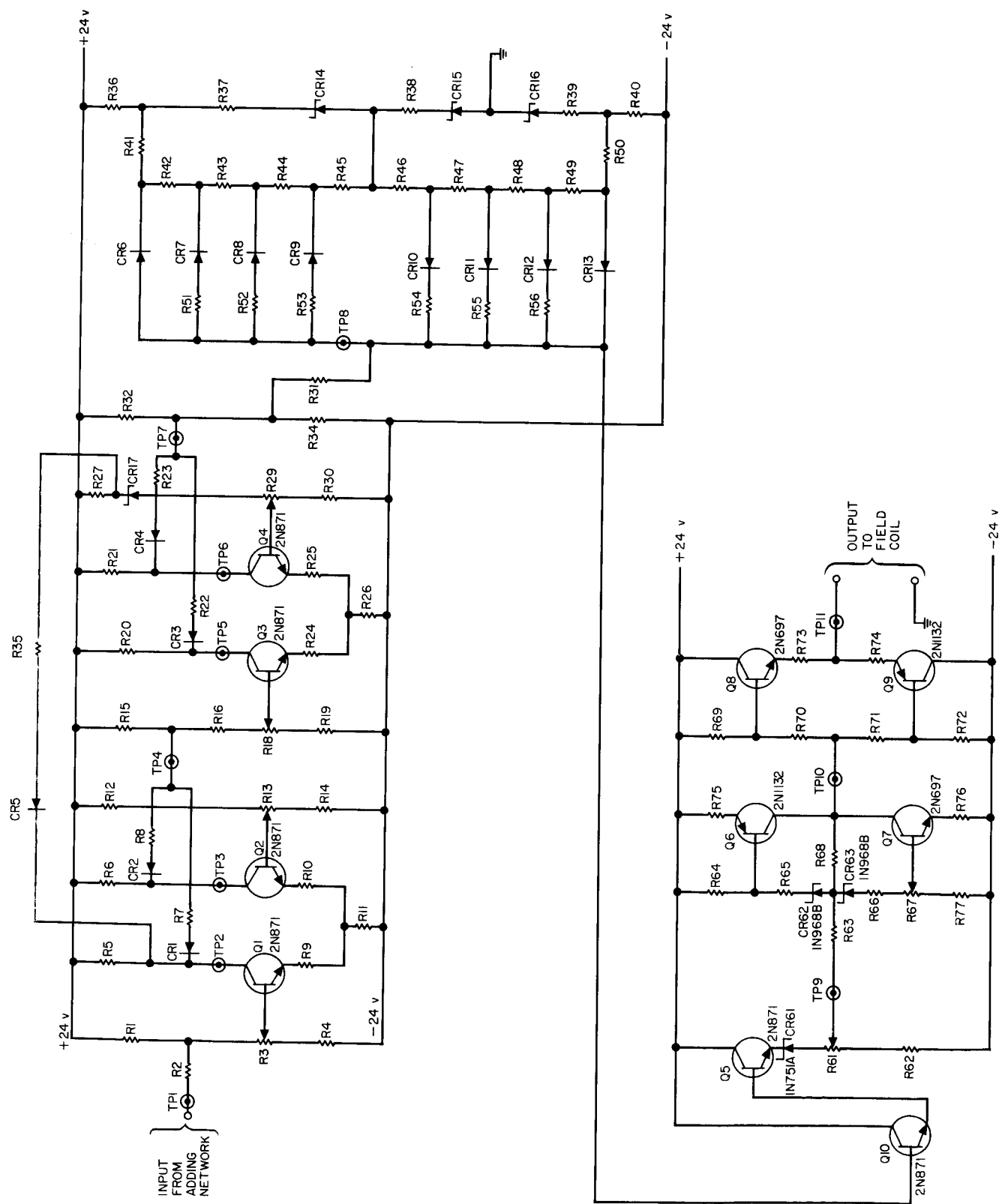


Figure 3-10. Waveform Generator and Power Amplifier

$$\begin{aligned}
e_1 &= E \sin (2 \pi f t) \\
e_2 &= E \sin (2 \pi f t + 22.5^\circ) \\
e_3 &= E \sin (2 \pi f t + 45.0^\circ) \\
e_4 &= E \sin (2 \pi f t + 67.5^\circ) \\
e_5 &= E \sin (2 \pi f t + 90.0^\circ) \\
e_6 &= E \sin (2 \pi f t + 112.5^\circ) \\
e_7 &= E \sin (2 \pi f t + 135.0^\circ) \\
e_8 &= E \sin (2 \pi f t + 157.5^\circ)
\end{aligned}$$

where the amplitude E is approximately 3.2 volts and the frequency f is approximately 1.67 cps. The phase angles of these eight voltages differ from each other by integral multiples of 22.5 degrees, which is 360 degrees/16. Each of these voltages is applied to the input circuits of two of the 16 waveform generators.

The 16 waveform generators, with their associated amplifiers, are required to deliver to the field coils the following 16 currents:

$$\begin{aligned}
i_1 &= I \cos 2 \pi [\sin (2 \pi f t)] \\
i_2 &= I \sin 2 \pi [\sin (2 \pi f t)] \\
i_3 &= I \cos 2 \pi [\sin (2 \pi f t + 22.5^\circ)] \\
i_4 &= I \sin 2 \pi [\sin (2 \pi f t + 22.5^\circ)] \\
i_5 &= I \cos 2 \pi [\sin (2 \pi f t + 45^\circ)] \\
i_6 &= I \sin 2 \pi [\sin (2 \pi f t + 45^\circ)] \\
i_7 &= I \cos 2 \pi [\sin (2 \pi f t + 67.5^\circ)] \\
i_8 &= I \sin 2 \pi [\sin (2 \pi f t + 67.5^\circ)] \\
i_9 &= I \cos 2 \pi [\sin (2 \pi f t + 90.0^\circ)] \\
i_{10} &= I \sin 2 \pi [\sin (2 \pi f t + 90.0^\circ)] \\
i_{11} &= I \cos 2 \pi [\sin (2 \pi f t + 112.5^\circ)] \\
i_{12} &= I \sin 2 \pi [\sin (2 \pi f t + 112.5^\circ)]
\end{aligned}$$

$$i_{13} = I \cos 2\pi [\sin (2\pi ft + 135.0^\circ)]$$

$$i_{14} = I \sin 2\pi [\sin (2\pi ft + 135.0^\circ)]$$

$$i_{15} = I \cos 2\pi [\sin (2\pi ft + 157.5^\circ)]$$

$$i_{16} = I \sin 2\pi [\sin (2\pi ft + 157.5^\circ)]$$

The amplitude I is approximately 37 milliamperes.

Operation. In the adding network (Figure 3-11), the output voltage e_1 is obtained by transmitting voltage e_a straight through the network without changing the phase angle. A similar statement applies to output voltage e_5 , which is obtained directly from voltage e_b . Each of the six other output voltages is obtained by combining two of the input voltages, after attenuating them to obtain the proper ratio of amplitudes to produce the desired phase angle of the resultant. For example, e_4 is obtained by attenuating voltage e_a through resistor R_1 , attenuating voltage e_b through resistor R_8 , and combining the two attenuated voltages for transmission through emitter-follower Q_4 to the output circuit. Resistor R_5 is a load resistor which is used for controlling the amplitude of the resultant voltage e_4 .

Figure 3-10 shows the circuits of one complete waveform generator and its associated amplifiers. The 1.67-cycle sine-wave input voltage is applied to the base circuit of transistor Q_1 through resistors R_2 and R_3 . In the figure, the numbers TP1, TP2, etc., designate test points, at which voltage waveforms are displayed on an oscilloscope. The voltage waveforms occurring at these various test points are represented in Figure 3-12, and are labelled with the numbers of the test points at which they occur. In the left-hand column, the curves are plotted as functions of time. In the right-hand column, the curves are plotted as functions of the input voltage at point TP1.

Transistors Q_1 and Q_2 of Figure 3-10 are employed in a push-pull Class A, linear amplifier circuit. The push-pull operation is obtained by means of resistor R_{11} , which is common to the two emitter circuits.

In Figure 3-12, the top left-hand curve represents the sine-wave input voltage at TP1 as a function of time. This voltage is applied through resistors R_2 and R_3 to the base circuit of transistor Q_1 .

The curves labelled TP2 and TP3 represent the ac output signal voltages across load resistors R_5 and R_6 , respectively. The collectors of Q_1 and Q_2 are connected to a full-wave rectifier comprising diodes CR_1 and CR_2 . By means of resistors R_{15} , R_{16} , R_{18} , and R_{19} , the anodes of these diodes are dc-biased in such a manner that diode CR_1 passes current during the negative half-cycle of the signal voltage at the collector of Q_1 and diode CR_2 passes current during the negative half-cycle of signal voltage at the collector of Q_2 . The dc bias is represented in Figure 3-12 by the horizontal line labelled E_{b11} .

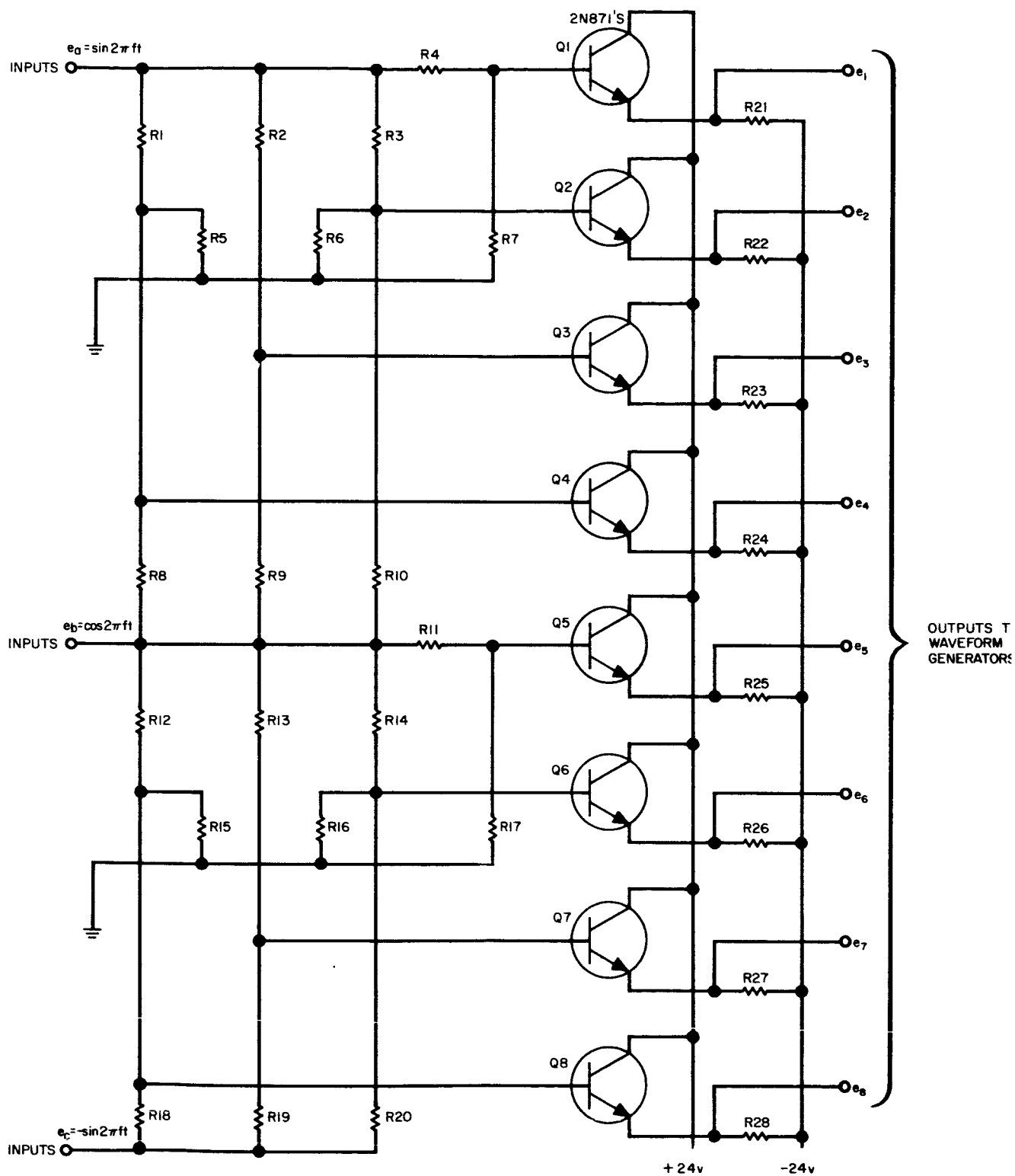


Figure 3-11. Adding Network

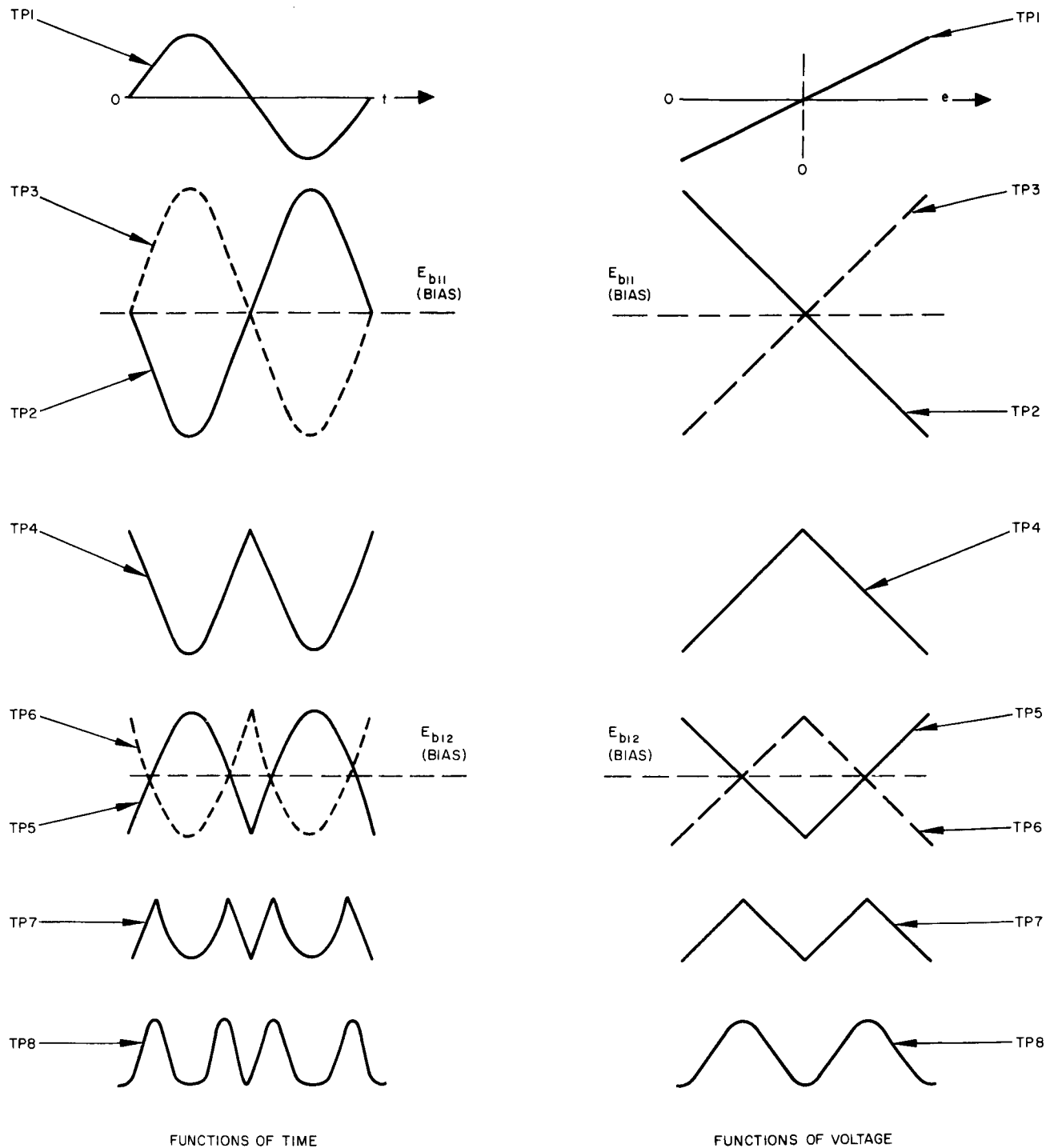


Figure 3-12. Voltage at Test Points (TPs) Waveform No. 1

The resultant output voltage of the full-wave rectifier is represented by the curve labelled TP4. It consists of a succession of identical half sine waves, in which one half-wave is received from Q1 and the next half-wave from Q2.

Transistors Q3 and Q4 of Figure 3-10 are used in a push-pull, Class A, linear amplifier, similar to that comprising Q1 and Q2. The signal voltages at TP5 and TP6 have the same form as the voltage at TP4 except that the signal voltage at TP5 is reversed with respect to the signal voltage at TP6, due to the push-pull action of the amplifier.

The collectors of Q3 and Q4 are connected to a full-wave rectifier comprising diodes CR3 and CR4. This rectifier is dc-biased, by means of resistors R32 and R34, at a voltage level halfway between the positive peak signal voltage and the negative peak signal voltage. This bias voltage is represented in Figure 3-12 by the horizontal line labelled E_{b12} . The diodes CR3 and CR4 transmit only those signal voltages which are negative with respect to voltage E_{b12} . The curve labelled TP7 shows the output voltage of these diodes.

In the right-hand curves shown in Figure 3-12, it can be seen that the voltage at TP7 is a symmetrical triangular wave when plotted as a function of the input voltage at TP1. Between TP7 and TP8, the signal voltage is modified in shape by means of a network consisting of diodes CR6 through CR13 and resistors R41 through R56. These diodes are biased by dc voltages in such a manner that they begin to draw current at various voltage levels, causing the output circuit of the full-wave rectifier to be loaded with additional shunt resistors as the signal voltage increases. This causes the output voltage to rise less rapidly, with the result shown in the bottom right-hand curve of Figure 3-12, in which the voltage is seen to be approximately a cosine function of the input voltage. Since this input voltage has the form $e = \sin(2\pi ft)$, the output voltage has the form

$$e_{11} = \cos 2\pi [\sin(2\pi ft)]$$

This is the form required for supplying current to the associated field coil.

In addition to the voltage e_{11} described above, it is necessary to generate another voltage,

$$e_{12} = \sin 2\pi [\sin(2\pi ft)]$$

Since the sine function is the same as the cosine function except for a 90-degree phase difference, the curves representing voltage as a function of input voltage for the sine function can be derived from the curves in the right-hand column of Figure 3-12 by shifting all these curves to the left. The

amount of this shift should correspond to one quarter-cycle of the voltage at TP8. The results of such a shift are shown in the right-hand column of Figure 3-13. The shift is obtained by adding a small constant to the independent variable. This constant is added by adjusting the dc bias voltage in the base circuit of transistor Q1 in the waveform generator used for generating e_{12} .

To make the waveform generator function over a wide enough range of input voltage for generating e_{12} , it is necessary to provide an additional bend in the curves labelled TP5 and TP6 in the right-hand column of Figure 3-13. This additional bend is labelled P3. The bend is obtained by means of elements CR5 and R35, shown in the schematic diagram. When the signal voltage across R5 varies in a negative direction beyond a certain level, current flows through diode CR5 and resistor R35, causing a voltage to be applied to the base circuit of transistor Q4. The voltage causes the downward bend at the point labelled P3. This downward bend causes the curve labelled TP5 in the left-hand column to sag between points P1 and P2 instead of being convex upward. A similar change occurs in the voltage at TP6.

In the power amplifier and driver shown in Figure 3-10, the signal passes through two cascaded emitter-followers, Q10 and Q5, which are necessary because the source impedance of the waveform generator is so much higher than the input impedance of the driver of the power amplifier. Transistors Q6 and Q7 are used in a push-pull, Class A, common-emitter, linear amplifier, which employs the complementary symmetry principle. This amplifier has inverse feedback, which is obtained by means of a voltage divider consisting of resistors R63 and R68. This inverse feedback is used for controlling the gain of the amplifier and for preventing drift of the dc bias voltage.

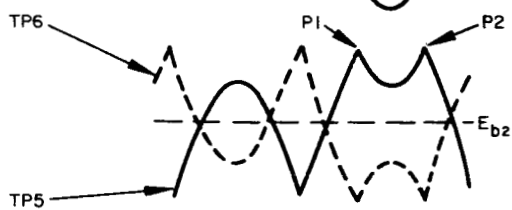
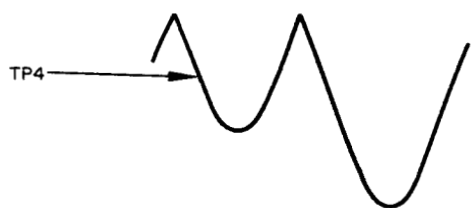
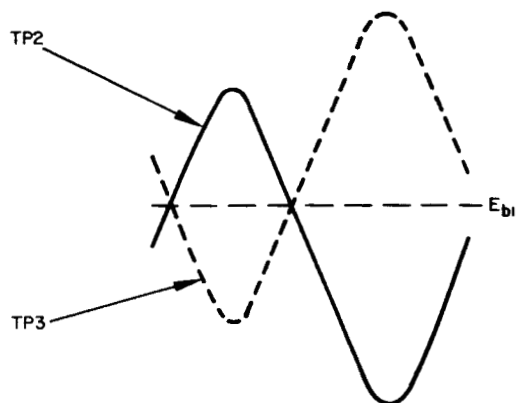
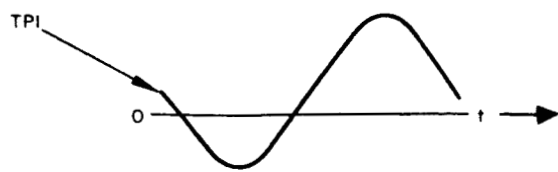
The output voltage of Q6 and Q7 is applied to the base circuits of the final amplifier stage, which uses transistors Q8 and Q9 in a Class AB, common-collector, linear amplifier, employing the complementary symmetry principle. This amplifier amplifies the signal current to a sufficiently high level for the corresponding field coil of the ferrite phase shifter.

Figure 3-14 shows oscilloscope patterns produced by the various voltages in an actual waveform generator. The various curves can be identified by the numbers TP1 through TP8.

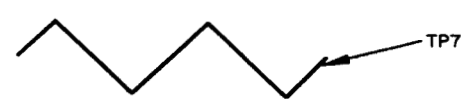
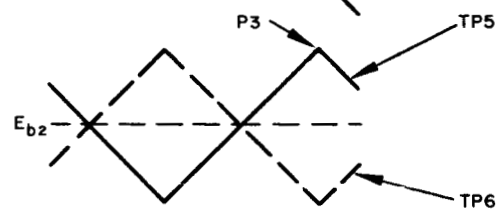
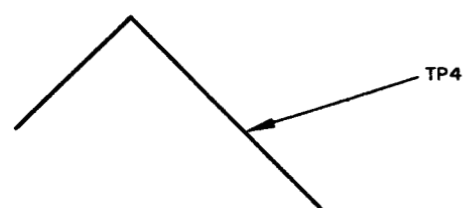
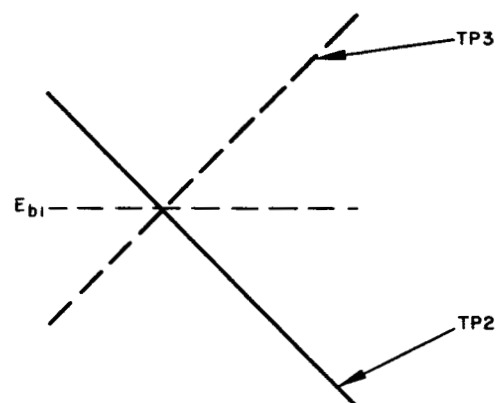
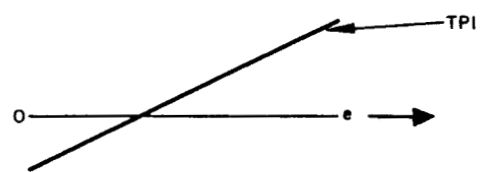
COLLINEAR ARRAY RECEIVING ANTENNA

Vertical Polarization

The receiving antenna consists of a collinear array of basic dipole elements series-fed by coaxial-line slots. An operating bandwidth of 203 mc centered at a frequency of 6301 mc is required. As reported last month, the use of a "flared-skirt" dipole basic element is being investigated. In this report period, the effect of variation in flare length has been measured. The

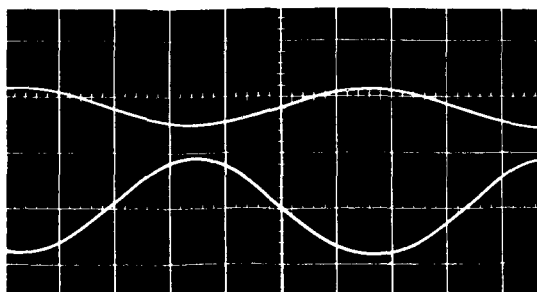


FUNCTIONS OF TIME

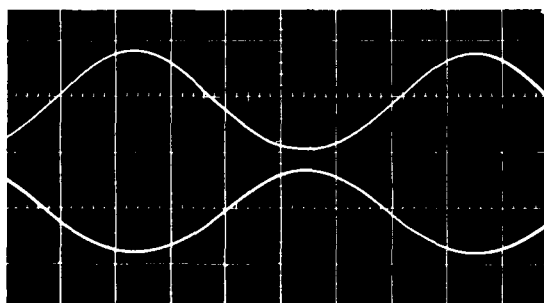


FUNCTIONS OF VOLTAGE

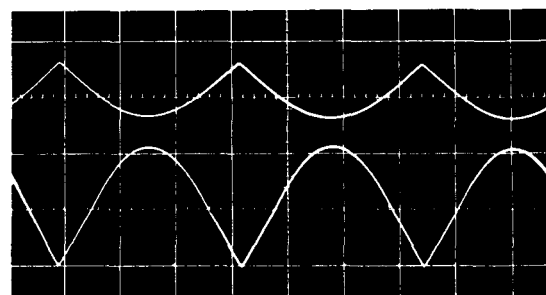
Figure 3-13. Voltage at Test Points (TPs) Waveform No. 2



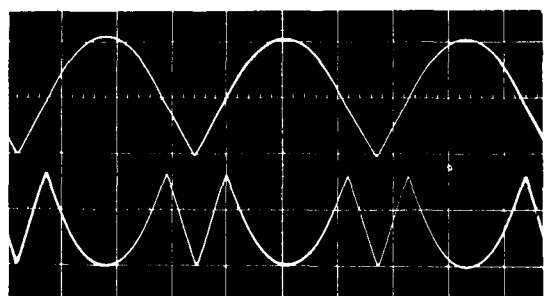
1) INPUT (TP1) 10 v/cm
COLLECTOR OF Q1 (TP2) 10 v/cm



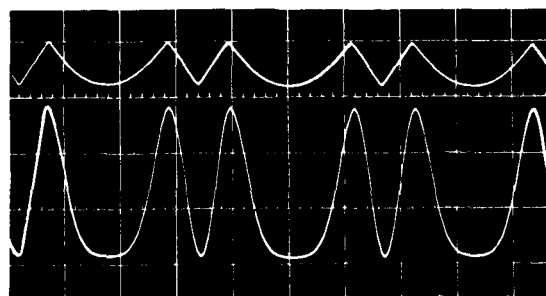
2) COLLECTOR OF Q1 (TP2) 10 v/cm
COLLECTOR OF Q2 (TP3) 10 v/cm



3) JUNCTION OF R7 AND R8 (TP4) 5 v/cm
COLLECTOR OF Q3 (TP5) 10 v/cm



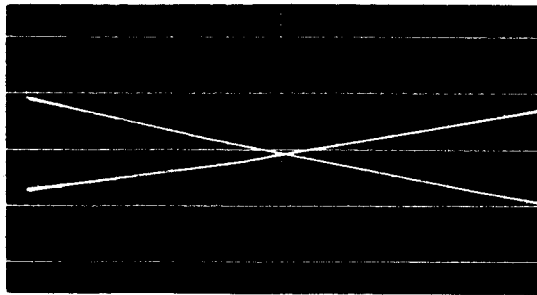
4) COLLECTOR OF Q3 (TP5) 10 v/cm
JUNCTION OF R22 AND R23 (TP7) 5 v/cm



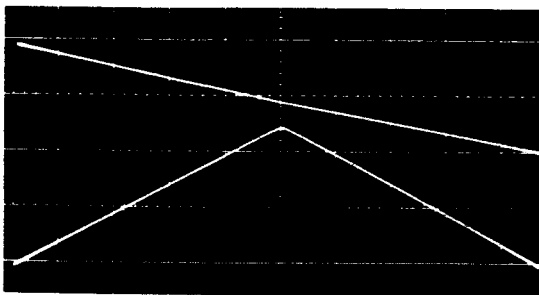
5) JUNCTION OF R22 AND R23 (TP7) 10 v/cm
JUNCTION OF R31 AND SHAPING NETWORK (TP8) 2 v/cm

a) Waveform No. 1, Independent Variable = Time

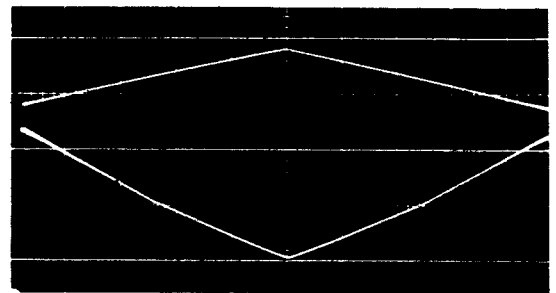
Figure 3-14. Measured Waveforms



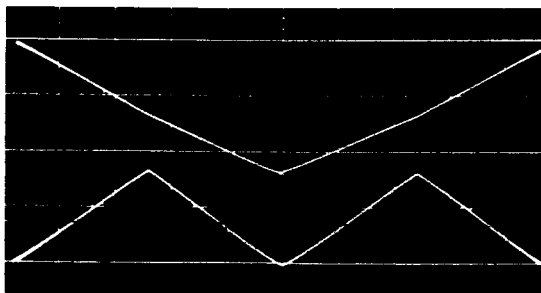
6) COLLECTOR OF Q1 (TP2) 10 v/cm
COLLECTOR OF Q2 (TP3) 10 v/cm



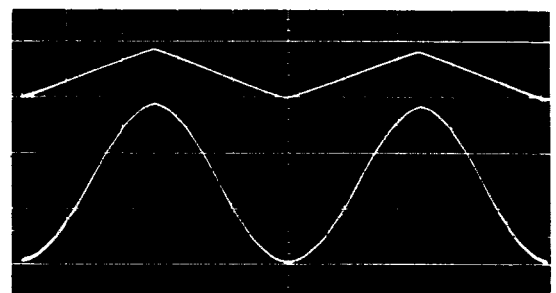
7) COLLECTOR OF Q1 (TP2) 10 v/cm
JUNCTION OF R7 AND R8 (TP4) 2 v/cm



8) JUNCTION OF R7 AND R8 (TP4) 5 v/cm
COLLECTOR OF Q3 (TP5) 10 v/cm



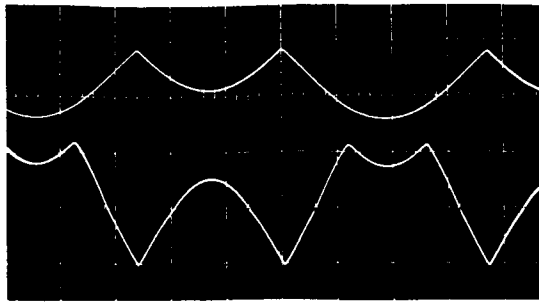
9) COLLECTOR OF Q3 (TP5) 10 v/cm
JUNCTION OF R22 AND R23 (TP7) 5 v/cm



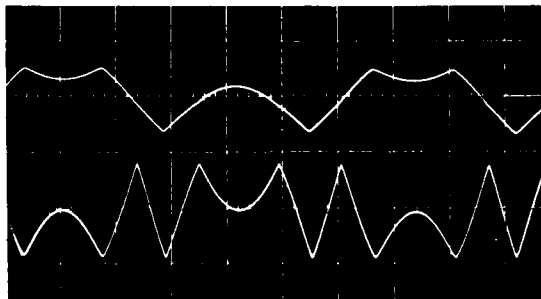
10) JUNCTION OF R22 AND R23 (TP7) 10 v/cm
JUNCTION OF R31 AND SHAPING NETWORK (TP8) 2 v/cm

Figure 3-14 continued. Measured Waveforms

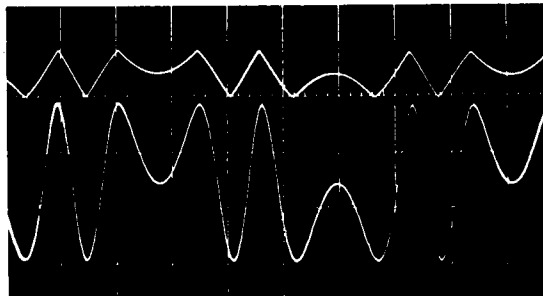
b) Waveform No. 1, Independent Variable = Voltage



11) JUNCTION OF R7 AND R8 (TP4) 5 v/cm
COLLECTOR OF Q3 (TP5) 10 v/cm



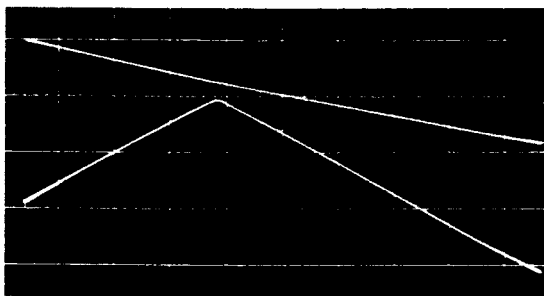
12) COLLECTOR OF Q3 (TP5) 20 v/cm
JUNCTION OF R22 AND R23 (TP7) 5 v/cm



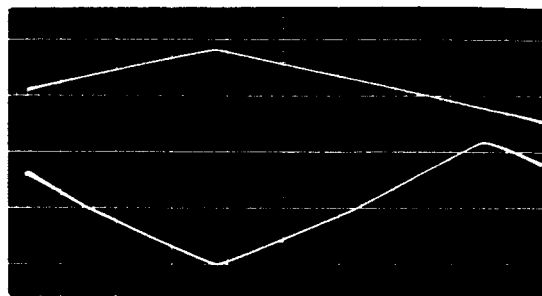
13) JUNCTION OF R22 AND R23 (TP7) 10 v/cm
JUNCTION OF R31 AND SHAPING NETWORK (TP8) 2 v/cm

Figure 3-14 continued. Measured Waveforms

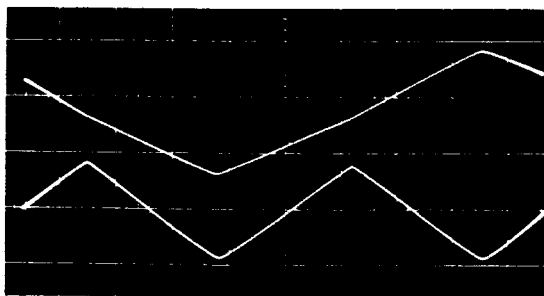
c) Waveform No. 2, Independent Variable = Time



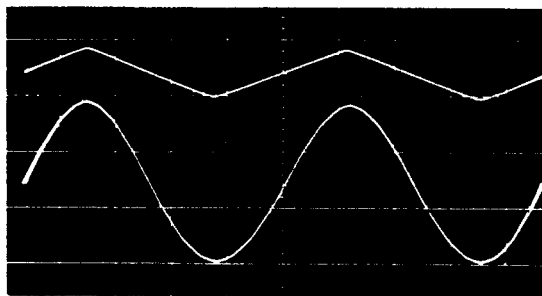
14) COLLECTOR OF Q1 (TP2) 10 v/cm
JUNCTION OF R7 AND R8 (TP4) 2 v/cm



15) JUNCTION OF R7 AND R8 (TP4) 5 v/cm
COLLECTOR OF Q3 (TP5) 10 v/cm



16) COLLECTOR OF Q3 (TP5) 10 v/cm
JUNCTION OF R22 AND R23 (TP7) 5 v/cm



17) JUNCTION OF R22 AND R23 (TP7) 10 v/cm
JUNCTION OF R31 AND SHAPING NETWORK (TP8) 2 v/cm

d) Waveform No. 2, Independent Variable = Voltage

Figure 3-14 continued. Measured Waveforms

results are given in Table 3-1 for several sets of values of dielectric constant of the bead material and gap spacing.

TABLE 3-1. IMPEDANCE OF FLARED-SKIRT DIPOLES

Frequency: 6200 mc; flare angle: 40 degrees

Insulating Material	Stycast HI K ($\epsilon_R=4$)		Plexiglass ($\epsilon_R=2.6$)	
Flare Length	Spacing			
	0.050 inch	0.200 inch	0.050 inch	0.200 inch
$0.250 \lambda_o$	0.36-j1.65	2.30-j1.95	0.33-j1.12	1.77-j1.08
$0.500 \lambda_o$	0.25-j1.60	1.40-j1.65	0.22-j1.02	1.09-j1.01
$0.750 \lambda_o$	0.32-j1.60	1.80-j1.75	0.23-j1.08	1.30-j1.00

The data shows that flair length did not materially affect the input impedance. However, a reduction in dielectric constant of the bead caused a reduction in the reactance component of impedance. The fact that further tests with a foam bead resulted in a still smaller reactive component indicates that the shape of the bead must be modified to obtain a pure resistive load to the feed line. Such modifications are now being made and a complete array is being constructed.

During the next report period, the optimum dimensions of the dielectric bead will be determined, and patterns of the array will be obtained.

A scaled version of the Syncom I transmitting array was fabricated and tested; it will serve as an interim receiving antenna for system tests. No attempt was made at an optimum performance design; consequently the gain is low (3 db) and the impedance match cannot be reduced to an acceptable level over the frequency band required. It will subsequently be replaced by the flared-skirt dipole array.

Horizontal Polarization

A horizontally polarized cloverleaf array is under development for possible application to the phased array transmitting antenna or to the collinear array receiving antenna.

A six-element cloverleaf array has been fabricated and tested (Figure 3-15). The elements were additive as shunt elements as expected; however,

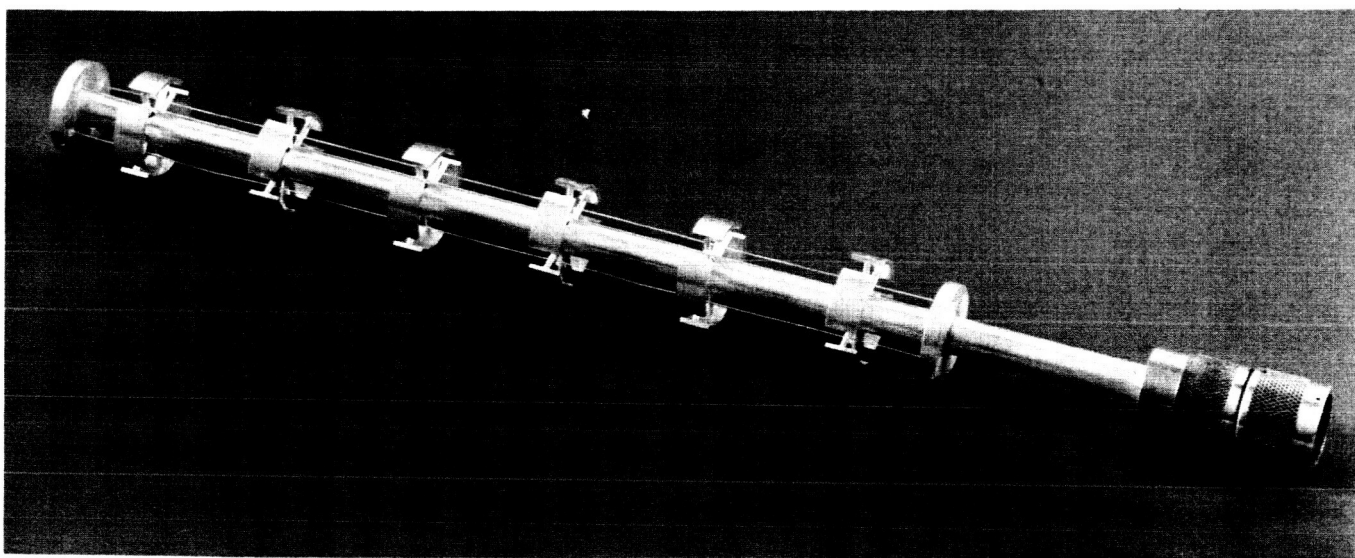


Figure 3-15. Six-Element Cloverleaf Array

the array was resonant at a frequency of 3830 mc instead of at the design frequency of 4080 mc. Figures 3-16 through 3-19 show E-plane and H-plane patterns at these two frequencies. The major characteristics of this array at the two frequencies tested are shown as:

<u>Characteristic</u>	<u>3830 mc</u>	<u>4080 mc</u>
VSWR	1.19:1	6.4:1
Omnidirectionality	0.3 db	1.8 db
Beamwidth	18.6 degrees	16.2 degrees
Sidelobe level	-9.7 db	-6.2 db
Gain	7.6 db (maximum)	1.7 db (minimum) 3.7 db (maximum)

At 4080 mc the presence of an "endfire" beam about 35 degrees from the axis of the array, down only 6.2 db from the broadside beam, indicates that the suppressor wires are not properly located. A method of obtaining a low VSWR over the desired frequency band has not been achieved as yet. The best impedance match obtained for the six-element array over a 150 mc band centered at 3830 mc is 1.8:1. This band is slightly greater than that which will be required if the cloverleaf array is scaled for use as the collinear array receiving antenna.

Plans for the next report period are: 1) to modify the six-element array to obtain resonance at 4080 mc; 2) to eliminate the endfire beam that occurs at 4080 mc; 3) to fabricate another six-element array for use with the present array, for mutual coupling measurements; and, 4) to continue the impedance matching effort.

STRUCTURE

A majority of the detail parts for the T-1 spacecraft structure have been constructed; Figure 3-20 shows a portion of these:

- 1) Panel attach tee
- 2) Solar panel stiffener
- 3) Quadrant electronics - package support
- 4) Thrust tube stringer
- 5) Large outer ring segment
- 6) Small outer ring segment

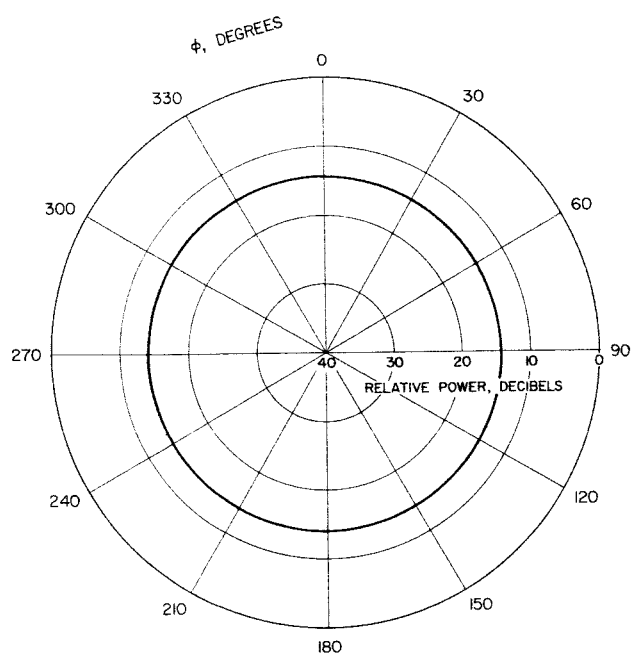


Figure 3-16. H-Plane 3830-mc Six-Element Cloverleaf Array

Gain = 7.6 db maximum

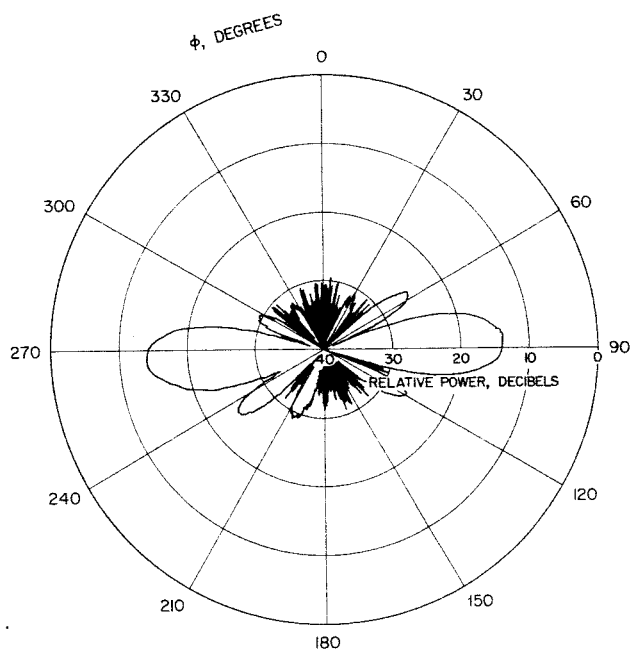


Figure 3-17. E-Plane 3830-mc Six-Element Cloverleaf Array

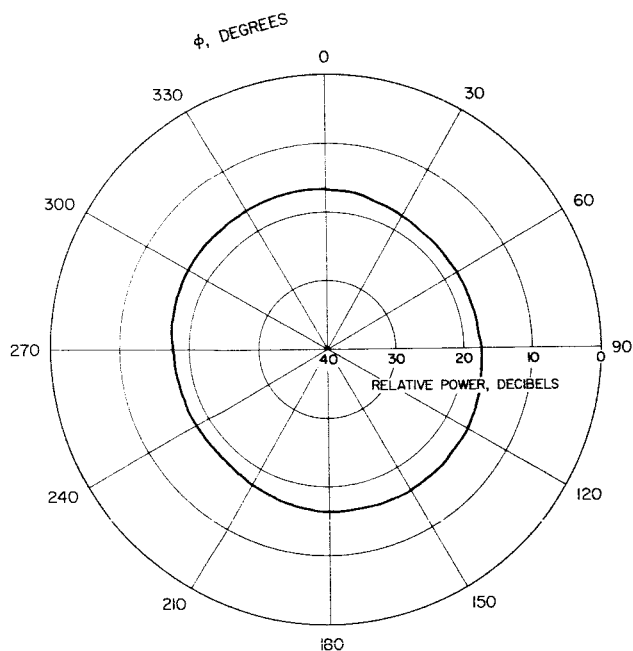


Figure 3-18. H-Plane 4080-mc Six-Element Cloverleaf Array

Gain = 1.7 db minimum
3.7 db maximum

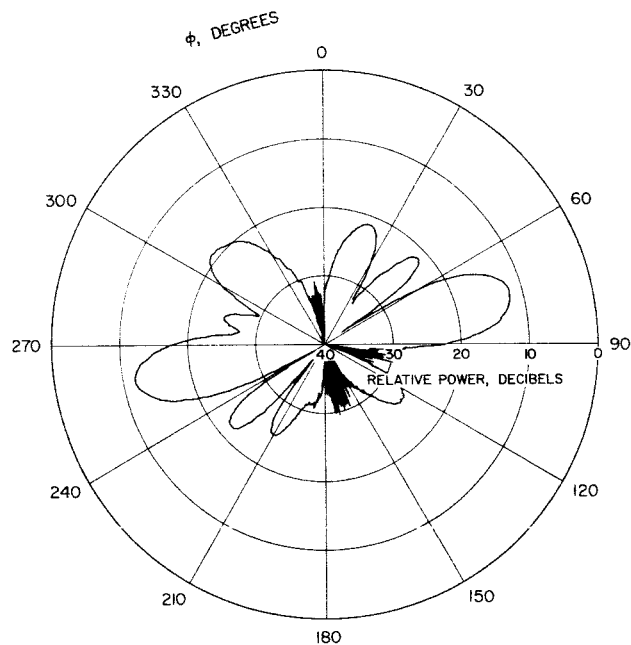


Figure 3-19. E-Plane 4080-mc Six-Element Cloverleaf Array

Figure 3-21 shows some of the parts in the aft subassembly:

- 1) Thrust tube stiffener ring
- 2) Thrust tube
- 3) Thrust tube ring

Figure 3-22 shows the thrust tube being assembled with the thrust tube ring, thrust-tube stiffener ring, and 12 stringers being held in place by the assembly fixture. Figure 3-23 shows the size comparison between the Syncom II thrust-tube and the entire Syncom I spacecraft.

The Lockheed drawing of the proposed spin-table was found to be in disagreement with the Hughes spacecraft design; however, this discrepancy was subsequently resolved. The spin direction will remain as originally planned, i. e. , clockwise (when looking at the transponder antenna end of the spacecraft).

Structural Analysis

All of the assembly drawings have been completed and fabrication initiated.

Due to NASA selection of a JPL apogee motor, modification of the present motor support points analysis will be made. The apogee rocket motor and bipropellant control system specifications are being reviewed for vibration requirements.

From a dynamic analysis viewpoint, an estimate of lateral frequency, using the analytical model, is expected by the end of the year. Influence coefficients obtained from the static test structure will be used to revise this estimate.

A structural design review is planned for 4 January 1963. Topics to be discussed include:

- 1) Design criteria
- 2) Stress analysis
- 3) Dynamic studies
- 4) Static and dynamic test plans
- 5) Manufacturing considerations

General Arrangement

Revisions of the quadrant electronics package space envelope have been made and released. Revisions to the structural drawings (to agree with

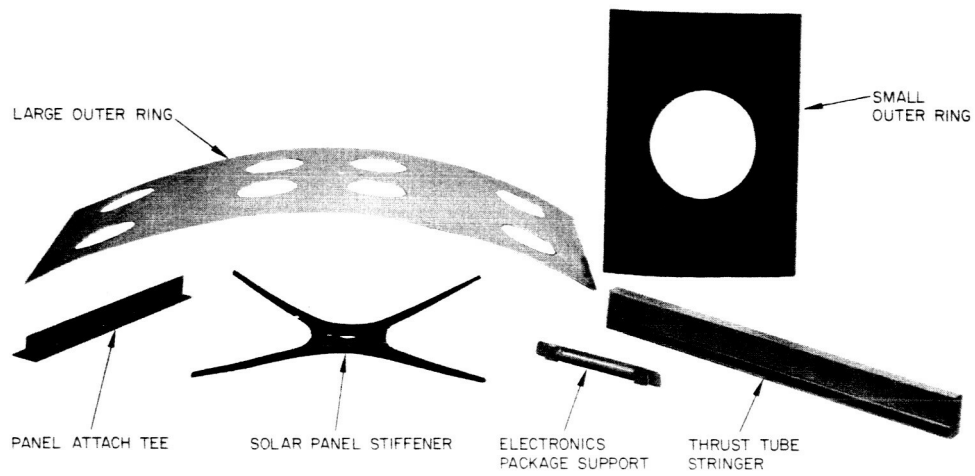


Figure 3-20. Syncom II Structure Details

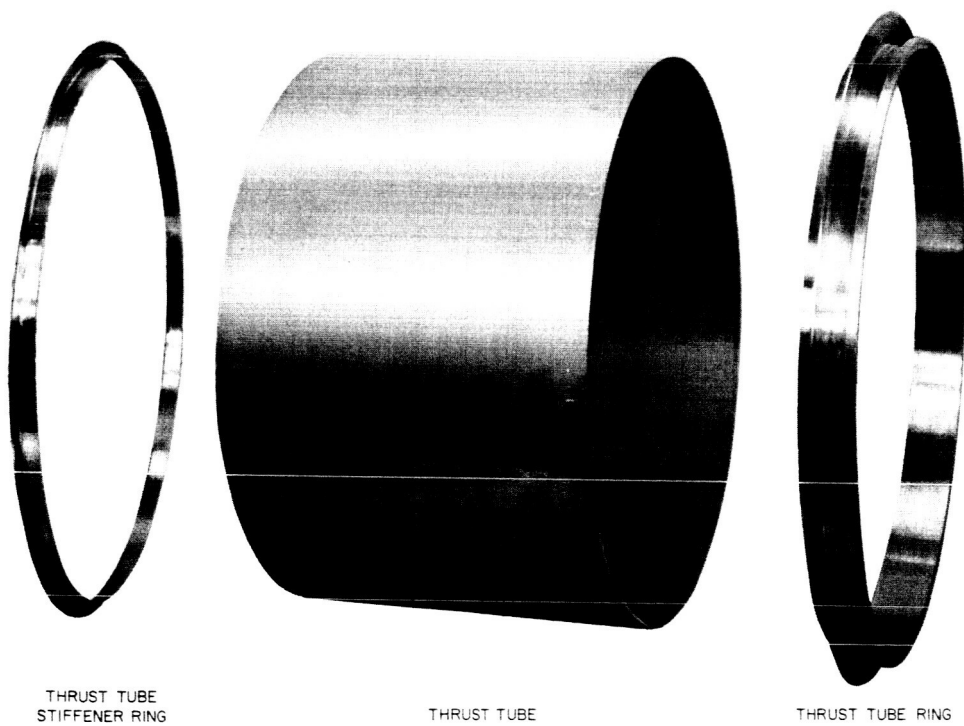


Figure 3-21. Exploded View of Thrust Tube

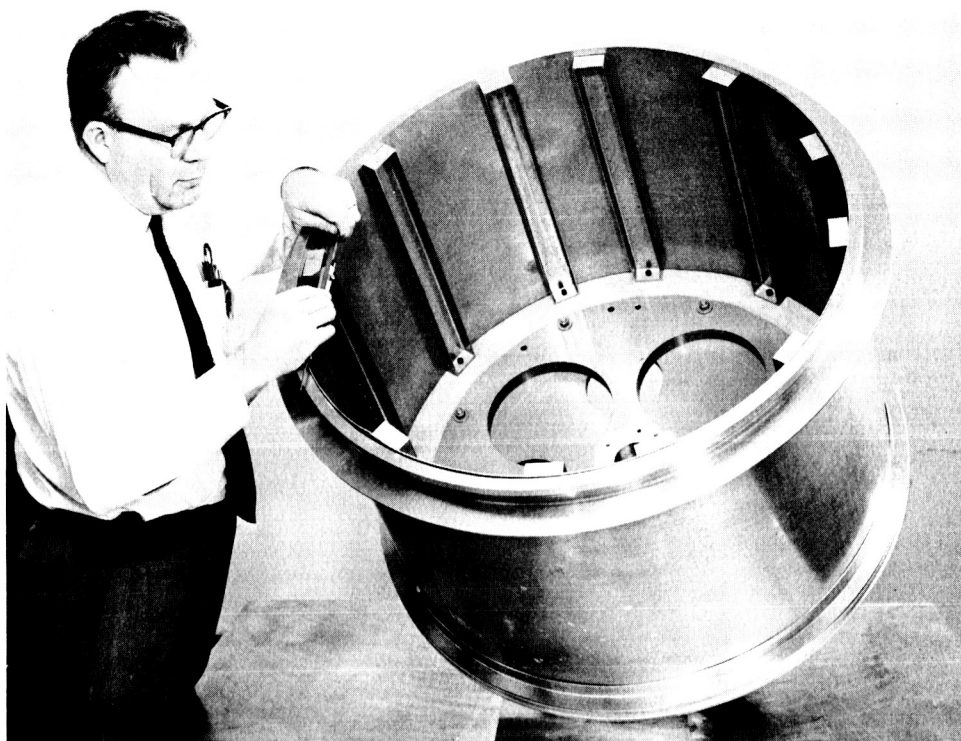


Figure 3-22. Thrust Tube Assembly



THRUST TUBE

SYNCOM I SPACECRAFT

Figure 3-23. Comparison of Size of Thrust Tube and Syncom I Spacecraft

the space envelope) are under way. The reason for these changes is to facilitate fabrication of the quadrant electronic packages.

Drawings for a dummy 30-inch spherical apogee motor had been completed but not released due to the nonspherical configuration of the JPL motor. Necessary revisions for the JPL cylindrical apogee motor are under way.

Weight Summary

The latest weight data for the spherical solid-propellant apogee motor configuration is summarized in Table 3-2. A detailed weight statement through final orbit condition is shown in Table 3-3.

Weight changes since the last weight statement are as follows:

<u>Change</u>	<u>Weight, pounds</u>
Battery packages and regulators — increase from 88 to 96 cells plus change from circular cylindrical to rectangular plate cells	+24.0
Latest estimate on solar panel supports, includes weight of stiffeners	-8.0
Spider assembly redesign	-1.7
Miscellaneous structural changes	+1.7

This report includes the weights of some detail parts in the aft structure, now in the process of assembly. These actual weights are in close agreement with the calculated weights for the same details.

Changes caused by replacement of the solid-propellant motor configuration from spherical to acylindrical shape will be reported.

HANDLING, WEIGHT, AND BALANCE EQUIPMENT

During the period, major effort was directed toward design and fabrication of assembly tooling. Main assembly stand and basic frame assembly tooling have been completed and are available for use pending delivery of the index head, which is due during the first week of the next report period. The fixtures designed to position and install stiffeners (Figure 3-24) will require minor redesign because of engineering changes; however, this will not cause any significant delay.



Figure 3-24. Aft Structure Assembly Fixture

TABLE 3-2. SYNCOM II ESTIMATED WEIGHT STATUS
Solid-Propellant Configuration

Subsystem	Δ Weight*	Weight, pounds	ϕ^{**}	θ^{***}		
Electronics	+16.0	130.0	0.244	0.097		
Wire harness		19.9	0.037	0.015		
Power supply		118.6	0.223	0.089		
Controls		38.6	0.072	0.029		
Propulsion		75.1	0.141	0.056		
Structure		131.3	0.247	0.098		
Miscellaneous		19.1	0.036	0.014		
		Weight, pounds	Z-Z	I_{Z-Z}	I_{X-X}	R/P
Final orbit condition		(532.6)	23.5	52.3	40.4	1.29
N ₂ pressurization		3.2				
N ₂ H ₃ -CH ₃ fuel		55.6				
N ₂ O ₄ oxidizer		92.4				
Total at apogee burnout		(683.8)	23.5	60.9	44.7	1.36
Apogee motor propellant		651.8				
Total payload at separation		(1335.6)	24.5	73.5	57.5	1.28
* = change in subsystem weight since last report.						
** = ratio of subsystem weight to final orbit condition weight.						
*** = ratio of subsystem weight to total payload at separation.						

TABLE 3-3. DETAILED WEIGHTS

Component	Δ Weight, pounds	Weight, pounds	
Electronic quadrants		80.0	
Telemetry transmitter		4.0	
Traveling-wave tube and converter		16.0	
Antenna electronics and supports		30.0	
Subtotal			130.0
Wire harness		19.9	
Subtotal			19.9
Battery packages	+24.0	75.8	
Solar cells		22.8	
Solar cell supports		20.0	
Solar panel stiffeners	-8.0	0	
Subtotal	+16.0		118.6
Fuel and oxidizer tanks		13.0	
Thrust chambers		3.6	
Thrust chambers		2.6	
Fill and vent valves		1.2	
Spin control assemblies		2.5	
Spin control assemblies		2.5	
Lines and fittings		2.0	
Miscellaneous		11.2	
Subtotal			38.6
Apogee motor installation		75.1	
Subtotal			75.1

TABLE 3-3 (continued)

Component	Δ Weight, pounds	Weight, pounds	
Thrust tube	+0.2	11.8	
Ring thrust tube	+1.4	6.3	
Ring stiffener		2.2	
Stringer tube	-0.4	8.0	
Spider assembly	-1.7	3.1	
Ribs		16.8	
Plate panel attachment		0.4	
Fitting panel attachment		2.2	
Ring, aft		3.4	
Bulkhead, aft		6.6	
Hardware and miscellaneous		1.3	
Panel assembly, btl		25.1	
Ring, outer, large	-0.1	5.3	
Ring, outer, small	+0.1	1.7	
Ring, inner	-0.2	4.4	
Support, electronics package	-0.1	0.9	
Support, electronics package	-0.1	0.3	
Hardware and miscellaneous		1.3	
Truss, jet		2.7	
Truss, sun sensor		2.3	
Truss, solar panel		4.5	
Bulkhead, forward		6.0	
Tee, panel attachment		2.4	
Support, electronics package	0.20	1.0	
Support, electronics package	-0.1	0.3	
Hoist fitting	+0.1	1.6	
Hardware and miscellaneous		1.3	
Hardware and miscellaneous		3.9	
Battery supports	0.9	4.2	
Subtotal			131.3

TABLE 3-3 (continued)

Component	Δ Weight, pounds	Weight, pounds	
Paint		3.0	
Thermal switch		4.5	
Nutation damper		2.0	
Miscellaneous		4.6	
Dynamic balance adjustment		5.0	
Subtotal			19.1

	Δ Weight, [*] pounds	Weight, pounds	Z-Z	I_{Z-Z}	I_{X-X}	R/P
Final orbit condition	16.0	532.6	23.50	52.32	40.40	1.29
N ₂ pressurization		3.2				
N ₂ H ₃ -CH ₃ fuel		55.6				
N ₂ O ₄ oxidizer		92.4				
Total at apogee burnout	16.0	683.8	23.50	60.89	44.69	1.36
Apogee motor propellant and expendables	15.3	651.8				
Payload at separation from booster	31.3	1335.6	24.48	73.46	57.50	1.28

The mobile assembly and test fixture, similar in design to the one successfully used with the Syncom I satellite, is approximately 60 percent complete in design. The spin test fixture design is proceeding on schedule. Final detail drawings are being prepared.

Design of the sling for handling the spaceframe and motor is also proceeding on schedule. It has been designed so that one basic sling using extra attachments will handle either or both the spaceframe or the motor.

HOT GAS REACTION JET CONTROL SUBSYSTEM

Evaluation of prospective contractors for the development of the hot gas reaction jet control subsystem continued during this report period. Four of the seven bidders were eliminated after comparison, on a point basis, of

management, cost, reliability, technical capability, etc. A more detailed investigation, including trips to the respective installations, resulted in elimination of a fifth competitor. The remaining two bidders met (separately) with Hughes to discuss deficiencies in their proposals. Re-proposals submitted by the two companies are currently being evaluated. Contract negotiations are expected on 18 January 1963.

The Statement of Work and Specification for this system have been revised to include the latest information available on system requirements. Changes made that have a significant effect on the subcontractor are: 1) reduction in the tank temperature range to 40° - 80°F (from 0° - 130°F), and 2) addition of the requirement for a spin control mechanism.

Spin-Rate Control Mechanism and Control System Design

Fabrication of the spin-rate control mechanisms has begun. Four complete assemblies will be made: the first will be used for performance and environmental tests; a second and third assembly will be available for spacecraft vibration tests; the fourth will be used for testing with the hot gas system. A viscous bellows damper has been assembled and is ready to be tested.

An analysis has been performed to determine both the effect of movements of the spin-speed control mechanism on spacecraft stability and the effects of spacecraft motions on the stability of the spin control mechanism. The coordinate system used in the analysis is illustrated in Figure 3-25.

Definition of Variables

$\bar{i}, \bar{j}, \bar{k}$	Unit vectors of spacecraft coordinate system; vector \bar{k} lies along positive spin axis.
$\bar{i}', \bar{j}', \bar{k}'$	Unit vectors along principal axes of spin-speed control mechanism; vector \bar{k}' lies in plane of symmetry through axial jet thrust axis; vector \bar{i}' is rotational axis of mechanism.
ℓ	Distance between spacecraft and spin control mechanism centers of gravity.
ρ	Distance from mechanism rotational axis to center of gravity of mechanism.
δ	Angle between \bar{k} and \bar{i}' .

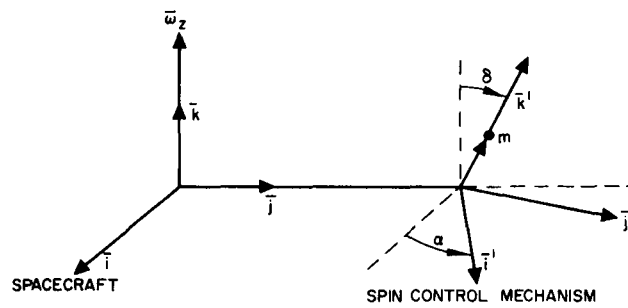


Figure 3-25. Coordinate Systems
Used in Analysis

α	Angle of rotation of mechanism rotational axis relative to normal line drawn from spacecraft radial line (in Figure 3-25 α is measured from vector \bar{i}).
\hat{I}, \hat{I}_z	Principal moments of inertia of the spacecraft, $\hat{I} = \hat{I}_x = \hat{I}_y$.
I, I_z	Principal moments of inertia of the spin control mechanism, $I = I_x' = I_y'$
m	Jet mass
T	Jet thrust
-	Bar over letter signifies that it represents a vector
H	Angular momentum

System Equations

Under the assumption that the spacecraft angular velocity component in the \bar{i}, \bar{j} plane is negligible compared to the spin velocity w_z , the \bar{i}' component of the angular momentum derivative for the spin control mechanism, for small δ , is ,

$$\begin{aligned}
 & - (I + m\alpha^2 + m\alpha l \cos \alpha) \ddot{\delta} - m\rho l \cos \alpha \dot{\delta}^2 \\
 & - \left[w_z^2 (I_{z'} - I) - m\rho^2 w_z^2 \right] \delta + m\rho l (-\dot{w}_z \sin \alpha + w_z^2 \cos \alpha) = \bar{H} \cdot \bar{i}'
 \end{aligned}
 \tag{3-1}$$

The restoring torques are due to a spring and viscous damper,

$$\bar{H} \cdot \bar{i}' = K(\delta - \delta_B) + D\dot{\delta}
 \tag{3-2}$$

where δ_B is the bias, or zero torque, position of the spring. Then the dynamic response of the mechanism is of the form

$$\begin{aligned}
& - (I + m_p \ell^2 + m_p \ell \delta \cos \alpha) \ddot{\delta} - (D + m_p \ell \dot{\delta} \cos \alpha) \dot{\delta} \\
& - \left[K + w_z^2 (I_{z'} - I) - m_p \ell^2 w_z^2 \right] \delta + K \delta_B \\
& + m_p \ell (-\dot{w}_z \sin \alpha + w_z^2 \cos \alpha) = 0
\end{aligned} \tag{3-3}$$

The roll torque exerted by the axial jet on the vehicle is

$$L_{\text{roll}} = - T \ell \sin \alpha \delta \tag{3-4}$$

Under ideal steady-state conditions, the roll torque output of the axial jet is zero when the vehicle spin speed w_z is at its design value \hat{w}_z . Thus from Equation 3-3 we have

$$\alpha_B = - \frac{m_p \ell \hat{w}_z^2 \cos \alpha}{K} \tag{3-5}$$

as the desired bias position of the spring.

Since the center-of-gravity displacements and moments of inertia of the spacecraft are negligibly affected by δ , the spacecraft roll equation of motion is simply,

$$\hat{I}_z \dot{w}_z = L_D + L_{\text{roll}} = L_D - T \ell \cos \alpha \delta \tag{3-6}$$

where L_D represents the disturbance torques arising from thrust misalignment of the axial and radial jets.

The roll-rate control system stability near steady state is studied by considering Equations 3-3 and 3-6. The following definitions and assumptions are required:

$$w_z = \hat{w}_z + r ; \dot{w}_z = \dot{r}$$

$$w_z^2 = \hat{w}_z^2 + 2r \hat{w}_z$$

$$m_p \ell \cos \alpha \delta \ll I + m_p \ell^2$$

$$\rho \delta < \ell_c \alpha$$

where r is the perturbed roll rate.

Equation 3-3 becomes

$$(I + m\rho^2) \ddot{\delta} + D\dot{\delta} + \left[K + \hat{w}_z^2 (I_{z'} - I) - m\rho^2 \hat{w}_z^2 \right] \delta + m\rho l \sin \alpha \dot{r} - 2 m\rho l \hat{w}_z \cos \alpha r = 0 \quad (3-7)$$

The thrust of the axial jet is either at the constant value T or zero. When the thrust is non-zero, we have, from Equation 3-6

$$\delta = \frac{L_D - \hat{I}_z \dot{r}}{T l \sin \alpha} \quad (3-8)$$

and from Equation 3-7

$$\begin{aligned} (I + m\rho^2) \hat{I}_z \ddot{r} + D \hat{I}_z \dot{r} + \left\{ \hat{I}_z \left[K + \hat{w}_z^2 (I_{z'} - I) - m\rho^2 \hat{w}_z^2 \right] - m\rho l^2 T \sin^2 \alpha \right\} \dot{r} + 2 m\rho l^2 T \hat{w}_z \cos \alpha \sin \alpha r \\ = L_D \left[K + \hat{w}_z^2 (I_{z'} - I) - m\rho^2 \hat{w}_z^2 \right] \end{aligned} \quad (3-9)$$

Thus, during thrusting periods the small perturbations from steady state are characterized by a third-order constant coefficient equation. Using Routh's criterion for analyzing the stability of the equation it is found that space-craft stability is ensured if

$$\begin{aligned} 1) \quad K > m\rho^2 \hat{w}_z^2 \\ 2) \quad D(K - m\rho^2 \hat{w}_z^2) > \frac{2m^2 \rho^3 l^2 T \hat{w}_z \cos \alpha \sin \alpha}{\hat{I}_z} \end{aligned}$$

Design values for the parameters indicate an extremely wide stability margin. For condition 1, the margin is about 23:1. Condition 2 requires that the damping force D be only greater than 2.32×10^{-6} ft-lb-sec. This corresponds to a damping coefficient ζ of 8×10^{-6} .

A disturbance torque forces the steady-state solution,

$$\delta = \frac{L_D}{T l \sin \alpha} \quad (3-10)$$

$$r = \frac{L_D \left[K + \hat{w}_z^2 (I_{z'} - I) - m \rho^2 \hat{w}_z^2 \right]}{2 m \rho \ell^2 T \hat{w}_z \cos \alpha \sin \alpha} \quad (3-11)$$

Clearly, the former must be within the unrestricted range of operation of δ , whereas the latter must be a permissible value of steady-state roll error.

When $T = 0$,

$$\dot{r} = \frac{L_D}{\hat{I}_z} \quad (3-12)$$

where L_D is the roll disturbance torque of the radial jet. The solution takes the form

$$r(t) = r(0) + \frac{1}{\hat{I}_z} \int_0^t \left[L_D(t) - T(t) \ell \sin \alpha \delta(t) \right] dt = f(t)$$

and we may regard

$$- m \rho \ell \sin \alpha \dot{r} + 2 m \rho \ell \hat{w}_z \cos \alpha r = g(t)$$

as a function of time. The perturbed roll system dynamical equation takes the form

$$(I + m \rho^2) \ddot{\delta} + D \dot{\delta} + \left[K + \hat{w}_z^2 (I_{z'} - I) - m \rho^2 \hat{w}_z^2 \right] \delta = g(t) \quad (3-13)$$

The stability of this second-order equation is assured if the signs of the coefficients of the characteristic equation are all positive and $D \neq 0$.

This requires that

$$K > m \rho^2 \hat{w}_z^2$$

The term $\hat{w}_z^2 (I_{z'} - I)$ is small and can be neglected. This is one of the criteria for the spacecraft stability consideration and as indicated, the stability margin is quite high, about 23:1. When $L_D = 0$, the steady-state solution is,

$$\delta = \frac{2 m \rho \ell \hat{w}_z \cos \alpha r}{K + \hat{w}_z^2 (I_{z'} - I) - m \rho^2 \hat{w}_z^2}$$

At least one spin-speed control assembly will be fabricated during January. It will be subjected to performance and environmental tests including centrifuge testing, vibration, and shock.

Testing of the viscous damper will be completed, plus any necessary redesigning. Parts will be procured for the final configuration.

APOGEE ENGINE LIAISON

The apogee engine for Syncom II will be GFE. JPL will supply the engine, which is considered a direct scale-up of the Syncom I apogee engine. NASA has asked that Hughes deal directly with JPL to resolve interface problems. A meeting was held with representatives of Goddard, JPL, and Hughes to establish preliminary engine design criteria and communication channels between Hughes and JPL.

The specification for the apogee engine was rewritten to incorporate changes recommended by NASA and JPL and to include recent changes in the expected engine environment.

4. NEW TECHNOLOGY

There were no items of new technology reported during the report period.

5. PROJECT REFERENCE REPORTS

- J. G. Lotta, "Syncom II Weight Report," ABL-248 Configuration, IDC 2243.11/20, 7 December 1962.
- D. C. Mead, "Syncom II Dual Mode Command Decoder," IDC 2941.20/69, 14 December 1962.
- Revised Preliminary Performance Specification, Syncom II Apogee Rocket Motor, 14 December 1962.
- M. J. Neufeld, "Revised Ascent Guidance Errors for Advanced Syncom" (Confidential), 19 December 1962.